Regional and sectoral contributions of NO$_x$ and reactive carbon emission sources to global trends in tropospheric ozone during the 2000-2018 period

5 Aditya Nalam [1,2,*], Aura Lupaşcu [2, **], Tabish Ansari [2], Tim Butler [1,2]

[1] Institut für Meteorologie, Freie Universität Berlin, Berlin, Germany

[2] Research Institute For Sustainability at GFZ Helmholtz Centre for Geosciences, Potsdam, Germany

[*] Now at Department of Atmospheric Physics, Faculty of Mathematics and Physics, Charles University, Prague, Czech Republic.

10 [**] Now at European Center for Medium Range Weather Forecast, Bonn, Germany

Correspondence to: Aditya Nalam (adinalam@zedat.fu-berlin.de)

Abstract. Over the past few decades, the tropospheric ozone precursor anthropogenic emissions: nitrogen oxides (NO$_x$) and reactive carbon (RC) from northern mid/high-latitude regions (North America (NAM), Europe (EUR) etc.), have been decreasing, and those from (sub)-tropical regions (South Asia (SAS), Middle-East (MDE), etc.) have been increasing,
15 leading to an equatorward emission redistribution. In this study, we quantify the contributions of various sources of NO$_x$ and RC emissions to tropospheric ozone using a source attribution technique during the 2000-2018 period in a global chemistry transport model. We tag the ozone molecules with the source of their NO$_x$ or RC precursor emission in two separate simulations: NO$_x$-tagged and RC-tagged. These tags include various natural (biogenic, biomass burning, lightning NOx and RC from methane oxidation), and regional anthropogenic precursor emission sources, and influx from stratosphere. We
20 simulate ~336 Tg O$_3$ of tropospheric ozone burden (TOB) with an increasing trend of 0.91 Tg O$_3$/yr (0.28 %/yr), largely contributed (and trend driven) by anthropogenic NO$_x$ emissions and methane oxidation. The ozone production efficiency of regional anthropogenic NOx emissions increases when emissions decrease (EUR, NAM etc.) and decreases when emissions increase (SAS, MDE, International Shipping etc.). Tropical regions, despite smaller emissions, contribute more to TOB compared to emissions from higher latitudes, consistent with previous work, predominantly due to large convection
25 (combined with intense sunlight and larger reaction rates) at the tropics thereby lifting O$_3$ and its precursor molecules into the free troposphere where ozone's lifetime is longer. We simulate a smaller relative contribution from tropical regions to the global mean surface ozone (GMS-O3) compared to their contribution to the TOB. The global population-weighted mean ozone (GPW-O3) is much larger compared to GMS-O3, mainly due to large anthropogenic emissions from densely populated regions: East Asia, South Asia, and other tropical regions, and a substantial contribution from international ship
30 NO$_x$ emissions. The increasing trends in anthropogenic precursor emissions from these regions are the main drivers of increasing GPW-O3.

Short Summary (500 Characters).

35   Tropospheric O_3 molecules are labelled with the identity of their precursor source to simulate contributions from various emission sources to the global tropospheric O_3 burden (TOB) and its trends. With an equatorward shift, anthropogenic NO_x emissions become significantly more efficient at producing O_3 and play a major role in driving TOB trends, mainly due to larger convection at the tropics effectively lifting O_3 and its precursors to the free troposphere where O_3 lifetime is longer.

1 Introduction

40   Tropospheric ozone is a major greenhouse gas (Myhre et al. 2013), after carbon dioxide and methane. It also has an indirect influence on the lifetime of methane through its impact on the hydroxyl radical, OH (Monks et al., 2015). At the surface, ozone is a major air pollutant causing a large number of premature deaths (~423100 Ozone attributable deaths [95 % confidence interval: 223200, 659400] in 2019; Malashock et al. 2022) and heavy yield losses in the production of staple food crops worldwide (losses of up to 79–121 Tg annually; Avnery et al. 2011, Mills et al. 2018). Tropospheric ozone initially thought to

45   be mostly of stratospheric origin (Junge, 1962), is also a secondary pollutant produced from the reaction between ozone precursor gases: nitrogen oxides (NO_x: NO and NO_2) and reactive carbon (RC: CH_4, CO and Volatile Organic Compounds (VOCs); Levy, 1972; Chameides and Walker, 1973; Crutzen, 1974). A multi-model assessment study showed that the tropospheric ozone burden has increased by ~44 % since the pre-industrial period, mainly driven by increasing anthropogenic emissions of ozone precursor gases (Griffiths et al., 2021). Gaudel et al., (2020) utilize the data from In-service Aircraft for a

50   Global Observing System database (IAGOS) and identify remarkable increase in tropospheric ozone since 1994 over several regions in the Northern Hemisphere. Addressing the effects of tropospheric ozone both as a pollutant and a greenhouse gas requires mitigation of the anthropogenic emissions of ozone precursors.

       Since 1980s, anthropogenic emissions of tropospheric ozone precursors from North America and Western Europe have

55   decreased in response to the implementation of control measures while the emissions from Asia, Central America, and Eastern Europe have increased due to economic and population growth (Granier et al., 2011, Cooper et al., 2014) leading to an equatorward shift in global emission pattern. A recent study (Li et al., 2024) confirms an equatorward shift in Asian NOx emissions between 2010 and 2017 according to bottom-up estimates. Zhang et al., (2016) found that this equatorward shift in precursor emissions is the dominant factor, compared to the change in magnitude of emissions and methane concentration,

60   that has led to an increase in the tropospheric ozone burden between 1980 and 2010. This is mainly due to larger convection of polluted air masses from the boundary layer into the free troposphere, in addition to larger reaction rates and NO_x sensitivity over the tropical regions (Wild et al., 2001) compared to extra-tropical regions. Further, Wang et al., (2022) show that increasing aircraft emissions play a major role in the increasing trend in tropospheric ozone burden over the 1995-2017 period. Similarly, the increase in methane concentration during the industrial period also had a substantial impact on tropospheric

65   ozone burden (Stevenson et al., 2013).

Source apportionment methods are used in chemical transport modelling studies to quantify the influence of specific emission sources on ozone concentration at any given location. Typically, global modelling studies have used two different methods for source apportionment: perturbation and tagging, which will be described in more detail below.

70

Several previous studies have used the perturbation method of source attribution to study the impact of emission changes from a particular region/sector on tropospheric ozone (e.g. West et al., 2007, Fiore et al., 2009, Jonson et al., 2018 etc). Zhang et al. (2021) use this method to study the influence of changing emissions from various world regions between 1980 and 2010 on tropospheric ozone burden. In their study, multiple model simulations were performed: one base simulation with all emissions at 2010 levels and other perturbed simulations with 1980 emissions from the region/sector of interest. The study found that the change in tropospheric ozone burden responded the most to perturbation in prescribed methane concentration. Of the geographical source regions, tropospheric ozone burden responded the most to perturbations in emissions of anthropogenic ozone precursor emissions at tropical regions: South Asian and Southeast Asian regions.

80

The second method of source apportionment is called tagging, which involves labelling the modelled ozone molecules with the name of its precursor emission sources. As opposed to the previously discussed perturbation method that delivers the sensitivity of simulated ozone to emission changes, this tagging method delivers the exact contribution to the simulated ozone concentration from each of the tagged emission sources (see Table 1 in Mertens et al., 2020 for a detailed comparison between the two methods). Several previous studies have implemented the tagging method in box (e.g., Butler et al., 2011, Coates and Butler, 2015), regional (Kwok et al., 2015, Lupascu and Butler 2019, Zhao et al., 2022), and global models (Grewe et al., (2010, 2017), Emmons et al., 2012, Butler et al., 2018) to study the contribution of various emission sources on ozone concentrations (see Butler et al., (2018) for a review of various tagging approaches). The formation of one tropospheric ozone molecule requires two precursors (NO_x and RC), a major challenge in its emission source attribution is to know the label of which of the precursors should the ozone molecule inherit.

90

Among the previous global modelling approaches that implement tagging, Grewe et al., (2010, 2017) calculate the production rate of the tagged ozone molecules, by giving equal weight to the proportion of tagged NO_x and RC molecules emitted from a given sector ("combinatorial" tagging). While this approach can deliver information on the role of each emission source in its contribution to the tropospheric ozone concentration, it does not communicate the contrasting roles of NOx and RC from those sources. For example, Mertens et al., (2018) using the combinatorial approach, attribute ~8 % of tropospheric ozone burden to ozone precursor emissions from land transportation but cannot determine which emitted precursor from land transportation: NO_x or RC contributes predominantly. Butler et al., 2018 formulated the tropospheric ozone source attribution system with tagging (TOAST) within the CAM4-Chem (Community Atmosphere Model version 4 with chemistry) model that requires running two separate simulations: NOx-tagged and RC-tagged, to separately attribute ozone to NO_x and RC sources respectively, by labelling them with the name of their originating source region/sector. With this approach, the previously

mentioned problems related to the contrasting roles of NO_x and RC, are avoided as the contribution from each precursor source is separately attributed. To illustrate: O_3 attributed to biogenic emissions in NOx-tagged simulation would clearly mean that the contribution is from emitted biogenic NO_x only, irrespective of where the RC comes from to produce the O_3 molecule. Contribution from biogenic RC emissions can be simulated in the RC-tagged simulation. In this way, the roles of NO_x and RC emissions from a given sector are exclusively simulated in separate simulations.

Butler et al., (2020) use the TOAST tagging technique to quantify the contribution of ozone precursor emissions for the year 2010 from several regions/sectors. They demonstrated that the ozone production efficiency can directly be calculated using this method, as the ratio of tropospheric ozone attributed to a tagged emission source to the amount of precursor emission from that source. NO_x emissions from tropical regions such as South Asia, Southeast Asia and Central America were found to be the most efficient at producing tropospheric ozone compared to the emissions from other regions, consistent with the earlier work of Zhang et al., (2016). They further showed using a methane perturbation introduced to NOx-tagged simulation, that the contribution to tropospheric ozone burden by NO_x emitted from international shipping increases especially strongly in response to changes in methane concentration.

While Butler et al., (2020) discuss the ozone precursor contributions to tropospheric ozone burden for one year: 2010, we use the TOAST tagging approach (further explained in section 2) in this study over the 2000-2018 period to answer the following questions: (i) In Sections 3.1 and 3.2: What is the contribution of precursor emissions from various regions/sectors to the global tropospheric O_3 burden? How do changes in these emissions during 2000-2018 affect their contribution to the trend in tropospheric ozone burden? (ii) Section 3.3: How does the ozone production efficiency (OPE) of ozone precursor emissions respond to the changes in these emissions during the 2000-2018 period? And (iii) in section 3.4: How do contributions of different ozone precursors to the tropospheric O_3 burden contrast with their contribution to global mean surface O_3 and population weighted O_3? We conclude our article with the summary, limitations, and future scope in section 4.

2 Methods

2.1 Simulation setup

We use the ozone source attribution methods described in Butler et al., (2018) and Butler et al., (2020). We perform simulations with CAM4-chem, which is a component of the CESM (Community Earth System Model) version 1.2.2 (Lamarque et al., 2012). The model is run at a horizontal resolution of 1.9º ×2.5º, with 56 vertical levels for the 2000-2018 period with specified dynamics from MERRA2 reanalysis (Molod et al., 2015). The temperature, horizontal winds, and sensible and latent heat fluxes from MERRA2 reanalysis dataset are nudged every time step (30 min) by 10 % towards analysis fields (i.e., a 5 h Newtonian relaxation timescale for nudging).

Anthropogenic emissions of NO_x, and non-methane reactive carbon (NMRC: CO, and volatile organic compounds (VOCs) collectively) including land-based emissions, international shipping emissions, and aircraft emissions are taken from Hemispheric Transport of Air Pollution version 3 (HTAPv3; Crippa et al., 2023) emissions inventory. We specify aircraft emissions at various altitudes effectively representing three different flight phases (landing/take-off, ascent/descent, and cruising). Biomass burning emissions are taken from GFED-v4 inventory (van der Werf et al., 2010). The biogenic NMRC emissions are taken from CAMS-GLOB-BIO-v3.0 (Sindelarova et al., 2021), and biogenic NO_x (from soil) is prescribed as in Tilmes et al., (2015). While we interpolate the emissions from HTAPv3's high-resolution dataset to our coarser model resolution, we also correct the interpolated land-based emissions over ocean grid cells by moving them to the nearest land grid cell (vice-versa for ocean-based emissions) to make sure that the emissions are allocated to the correct region for the source attribution.

We impose methane concentration as a surface boundary condition. The methane concentration is taken from the 2000–2018 average mole fraction fields from the CAMS CH_4 flux inversion product v18r1 (https://ads.atmosphere.copernicus.eu/cdsapp#!/dataset/cams-global-greenhouse-gas-inversion?tab=overview) and is specified as a zonally and monthly varying transient boundary condition. As in Butler et al., (2018) and Butler et al., (2020), we use the MOZART-4 chemical mechanism (Emmons et al., 2012) further modified to include tagged ozone tracers. This tagging system allows attribution of tropospheric ozone to reactive nitrogen (NO_x) and reactive carbon (CH_4 and NMRC) precursors in two separate simulations. Additionally, stratospheric influx as well as other minor production pathways of tropospheric ozone are also tagged in our model. For a complete attribution, we perform two separate simulations: (i) NOx-tagged; and (ii) RC-tagged (reactive carbon tagged) with their respective tagged emission sources.

We specify separate tag identities for biogenic, biomass burning, aircraft and surface-based anthropogenic emission sources of ozone precursors, and for ozone from production in the stratosphere. We tag anthropogenic emissions according to the HTAP Tier 1 regions (Galmarini et al., 2017) from which the respective NO_x or NMRCs are emitted. We focus our study on the northern hemispheric anthropogenic emissions by individually tagging the major northern hemispheric regions (East Asia, South Asia, North America, Europe, Middle East, and Russia-Belarus-Ukraine), and combining the other regions under the "Rest of the World" tag. Within our "Rest of the World" tag, some regions (e.g. Central Asia, Southeast Asia etc.) have been explicitly tagged in our NOx-tagged simulation but not in our RC-tagged simulation. We also specify additional tags for emissions from international shipping and aircraft emissions (see Table 1 and Fig. S1 for a summary of tags used in this study).

We specify an additional tag for NO_x emission from lightning in our NOx-tagged simulation, and for RC from methane oxidation in our RC-tagged simulation. In both NO_x and RC tagged simulations, the sum of tagged ozone tracers is equal to the total ozone simulated by the model.

2.2 Model Evaluation

CAM4-Chem has been evaluated in previous studies for simulating tropospheric ozone and precursors (Lamarque et al., 2012, Tilmes et al., 2015), and was also evaluated in its ozone-tagged configuration by Butler et al., (2018) and Butler et al., (2020). Here we evaluate the configuration of CAM4 Chem used in this study, which primarily differs from the earlier work though its use of the HTAPv3 global emissions. In Fig. 1 we compare our simulated surface ozone against gridded observation dataset provided by Tropospheric ozone assessment report (TOAR; Schultz et al., 2017) until year 2014. We also make the comparison using simulation output from "CESM2-WACCM6" model which is part of the CMIP6 ensemble (Emmons et al., 2020), using this as a standard reference model. Results are shown as monthly averages over various HTAP Tier 2 regions (Galmarini et al., 2017) at the grid cells where the TOAR data is available. We overestimate the surface ozone mixing ratio by up to ~4-12 ppbv over most regions where TOAR data is available, largely during the summer months. This overestimation is also simulated by CESM2-WACCM6 model (shown in Fig.1) and is consistent with high model bias of ~7 ppbv simulated by most models in various ensembles, as discussed in Young et al., (2018). We also simulate an underestimation of up to 2-6 ppbv over northern and eastern united states during winter months, which is not simulated by CESM2-WACCM6. For the year 2010, we simulate slightly smaller surface ozone at most regions over grid cells where TOAR data is available compared to that simulated by Butler et al., (2020), and is closer to the observations from TOAR dataset.

We evaluate free tropospheric ozone against the ozone sonde-based climatology compiled by Tilmes et al., (2012). Figure 2 shows the comparison our simulated climatology (2000-2010) to the ozone sonde climatology (1995–2010) in Taylor-like diagrams (Taylor, 2001; Tilmes et al., 2012) at 900, 500, and 250 hPa pressure levels, grouped by latitude ranges. The correlation coefficient between the observed and simulated monthly regional O_3 average is usually more than 0.8, and the fractional mean difference is usually within 25 % at most regions in the troposphere. The model captures the vertical distribution of ozone derived from ozone sonde climatology very well, although slightly biased high particularly in the upper troposphere at most sites (Fig. S2). Our free troposphere evaluation results are therefore largely consistent with previously evaluated versions of CAM4-Chem (Tilmes et al., 2012, Zhang et al., 2016, Emmons et al., 2020).

2.3 Trend Analysis

We express the trend for the 2000-2018 period in various quantities discussed in our study: Precursor emissions, tropospheric ozone burden, global surface mean and population-weighted mean ozone concentration as a slope of the timeseries in respective units/yr, and in %/yr relative to the first absolute value (for year 2000). This slope is calculated using the Theil-Sen estimator method available as a python module (https://docs.scipy.org/doc/scipy/reference/generated/scipy.stats.theilslopes.html), which also calculates the 95 % confidence interval of the slope. We further use the Mann-Kendall test to determine the extent to which the detected trend is monotonic

(Hussain and Mahmud, 2019), expressed by the p-value. In the TOAR Guidelines for best statistical practices (Chang et al., 2023), it is recommended not to use a dichotomized expression such as significant/insignificant trend. Hence, we also provide the p-value and the 95 % confidence interval in the supplementary information for the interested readers to assess the meaningfulness of the estimated trend in our study. For the sake of discussion in sections 3 and 4, we categorize the trends with p-values less than 0.05 to be of high certainty, between 0.05 and 0.1 to be of medium certainty and larger than 0.1 to be of low certainty (Table 3 in Chang et al., 2023).

3 Results

We discuss our results related to the ozone precursor emissions, contribution to tropospheric ozone burden, ozone production efficiency, and contribution to surface mean and population-weighted mean ozone from each of the tags used in our study. Each subsection is further divided into two parts to discuss the role of NO_x and RC tagged contributions separately. All our results are discussed as timeseries of annual means for the 2000-2018 period, unless otherwise specified. When referring to anthropogenic emissions and their contributions to tropospheric ozone in our discussion, we only refer to surface-based anthropogenic emissions and exclude aircraft emissions.

3.1 Ozone precursor emission trends

3.1.1 NOx emissions

Table 2 shows the global NO_x emissions (averaged over the 2000-2018 period) from various regions and sectors, and their relative contribution (in %) to the total NO_x emissions. Fig. 3 (a and c) shows the time-series of NO_x emissions from all sources: natural/global sources (a), and regional anthropogenic sources (c).

Over the period 2000-2018, the average annual NO_x emissions are ~49 TgN/yr, which includes both surface and aloft emissions. There is an increasing trend with medium certainty in the total NO_x emissions over the 2000-2018 period, with ~46.6 TgN/yr emitted in 2000, peaking at ~51.3 TgN/yr in 2011 and decreasing to ~48.2 TgN/yr emitted in 2018 (Fig. 3(a); Table 3).

The trend in total NO_x emissions is mainly driven by the anthropogenic NO_x emissions which are the largest source of NO_x (~35.6 TgN/yr (72.5 %); Table 2), much larger than natural sources such as lightning, biomass burning and biogenic emissions which contribute by ~7.1, 8.5 and 10 % respectively (Table 2). We also notice a slight decrease in the global anthropogenic NO_x emissions in 2008-2009, mostly related to the global financial crisis (Schneider and van der A 2012).

225 Among the anthropogenic NO_x emissions, East Asian emissions are the largest (~18.5 %; Table 2), with an increasing trend with high certainty (~0.25 TgN/yr; Table 3 and Fig. 3) over the 2000-2018 period. These emissions increase at 0.49 TgN/yr^2, peak in 2011 and start declining after that at -0.44 TgN/yr^2 (Zheng et al., 2018), as shown in Fig. 3c and Table S2, which largely explain the timeseries of anthropogenic and total NO_x emissions timeseries shown in Fig. 3a. The NO_x emissions increase over South Asia (0.13 TgN/yr^2), Middle East (0.06 TgN/yr^2) and "Rest of the world" (0.15 TgN/yr^2), whereas they

230 decrease over North America (-0.33 TgN/yr^2), Russia-Belarus-Ukraine region (-0.02 TgN/yr^2), and Europe (-0.11 TgN/yr^2). The magnitude of international ship NO_x emissions (4.04 TgN/yr) is comparable to that of NO_x emissions from continental regions such as North America, Europe, and South Asia (Table 2), and have an increasing trend (~0.08 TgN/yr^2; Table 3) with high certainty. These trends effectively also indicate an overall equatorward shift in anthropogenic emissions as discussed in several previous studies (e.g., Zhang et al., 2016, Gaudel et al., 2020, Zhang et al., 2021). We further illustrate this equatorward

235 shift using zonal sum profiles of deviation in anthropogenic NOx emissions from year 2000 (Fig. S4a). The zonal NO_x emissions relative to year 2000 show a positive (negative) deviation south (north) of ~35ºN latitude, indicating an equatorward shift in the overall global NOx emissions.

Emissions from the aircraft sector contribute only 0.93 TgN (~1.90 %) to the total NO_x emissions, with an increasing trend of

240 ~2.5 %/yr. This is comparable to the emissions taken from CEDS inventory reported by Wang et al., (2022): 0.88 TgN (contributing ~3.3 % to total NO_x emissions) increasing at ~3.46 %/yr between 1995 and 2017.

3.1.2 Reactive Carbon emissions

The total amount of tropospheric reactive carbon emissions averaged over the 2000-2018 period in our simulations is ~1342 TgC/yr (Table 4) with small increasing trend (0.25 %/yr^2; Table 5) (Fig. 3(b)). Methane and biogenic NMRCs are the largest

245 sources of reactive carbon (each about ~430 TgC (32 %); Table 4; Fig. 3b; Heald and Kroll 2020). Total anthropogenic NMRC emissions contribute ~302 TgC/yr (~22.5%; Table 4) and Biomass burning emissions contribute ~171 TgC/yr (~12.8 %). Aircraft emissions contribute very small amounts (Table 4).

Since the concentration of methane is fixed at the surface in our simulations, we consider the methane oxidation rate derived

250 from methane's oxidation reaction with atmospheric hydroxyl radical as the effective source of RC for subsequent ozone production through rapid chemical reactions. We simulate ~438 TgC/yr of methane oxidation with an increasing trend of high certainty over the 2000-2018 period. The prescribed CH_4 concentrations are such that there is a plateau until the year 2006 (Lan et al., 2024) followed by a steep increase (Fig. 4a: red line). Our simulated methane oxidation rate also increases with high certainty but does not strictly follow this plateau followed by steep increase pattern and has large inter-annual variability

255 (Fig. 4a). This could possibly be due to variability in the prescribed meteorology and OH concentration (Fig. 4b) resulting in variations in the oxidation rate of methane. We simulate slightly larger methane oxidation for the year 2010 compared to that

simulated by Butler et al., (2020), possibly due to the usage of a different anthropogenic emissions dataset, prescribed CH_4 mixing ratio and prescribed meteorology dataset. A detailed comparison of methane related variables such as prescribed concentration, burden, lifetime, oxidation rate etc., between our study and Butler et al., 2020 for the year 2010 is provided in

260 Table S4. While the absolute contributions from methane oxidation, anthropogenic and biogenic NMRC emissions to total reactive carbon emissions increase with medium-high certainty (Fig. 3b), their relative contributions show trends with low certainty (Supplementary Figure S3b)

The tropospheric methane lifetime (~8.54 years), calculated as the total atmospheric methane burden divided by tropospheric

265 methane oxidation rate, decreases with high certainty (-0.01 years/yr; Table S5) in our simulations (Fig. 4a: Magenta line). This result is contrary to the expectation that methane lifetime might increase due to increasing methane concentrations leading to a smaller availability of OH radicals to oxidize methane (Prather et al., 1996). CH_4 oxidation with OH radical being the major loss pathway for CH_4, we show the time-series of OH in Fig.4b. Here we simulate an increasing trend in air-mass-weighted tropospheric OH concentration (a prominent indicator for tropospheric oxidizing capacity; e.g., Voulgarakis et al.,

270 2013, Chua et al., 2023) but with low certainty. Nevertheless, the CH_4-reaction-weighted tropospheric OH concentration (Lawrence et al., 2001) shows an increasing trend with high certainty. This increasing trend in tropospheric OH concentration is consistent with the trend discussed in Chua et al., (2023) and explains the decreasing lifetime of CH_4 as these quantities are inversely proportional. The increasing OH availability despite increasing CH_4 concentration could be due to increasing NO_x emissions over the simulated period that recycle HO_2 to OH (e.g. Lelieveld et al., 2008; Chua et al., 2023). The mean magnitude

275 of our air-mass-weighted tropospheric OH concentration (~12.7 * 10^5 molec/cm^3) is slightly larger than previous studies (~10.8 * 10^5 molec/cm^3 in Chua et al., 2023 or ~11.7 * 10^5 molec/cm^3 in Voulgarakis et al., 2013) which is likely why we simulate a mean CH_4 lifetime slightly smaller than the aforementioned studies (~9 years), but within the multi-model range (7.1-10.6 years) reported in Voulgarakis et al., (2013).

280 Among the anthropogenic NMRC emissions, East Asian emissions are the largest (~95.4 TgC/yr (7.11 %); Table 4), increasing at 3.54 TgC/yr^2 peaking in 2011 and decreasing after that at -2.82 TgC/yr^2(Fig. 3(d); Table S6), a feature similar to the NO_x emissions. Second largest emitter is the "Rest of the World" region (~90.8 TgC/yr (6.76 %); Table 4), with an increasing trend of high certainty (Fig. 3 (d)). Remaining regions each contribute to less than 5 % of reactive carbon emissions. South Asian, Middle Eastern, and ship NMRC emissions show an increasing trend, and North American, European, Russia-Belarus-Ukraine

285 region's NMRC emissions show a decreasing trend (Fig. 3 (d); similar sign of trend also seen for anthropogenic NOx emissions). We also see an equatorward shift in global anthropogenic NMRC emissions, similar to the anthropogenic NO_x emissions in our zonal sum profiles of deviation in anthropogenic NMRC from year 2000 (Fig. S4b).

3.2 Tropospheric ozone burden

The tropospheric ozone burden is calculated as the mass of ozone in the model grid cells below the ozone-tropopause, defined as the highest layer in the upper troposphere with an ozone mixing ratio less than 150 ppb (E.g., Bak et al., 2022, Liu et al., 2022). We simulate a climatological average tropospheric ozone burden of ~318 Tg O_3, with an increasing trend of 0.72 Tg O_3/yr over the 2000-2018 period. Our simulated tropospheric ozone burden is towards the lower end of values simulated by several multi-model studies for the 2005-2014 period (values from Griffiths et al., 2021): the CMIP 6 ensemble 356±31 Tg O_3; ACCENT: 336 ± 27 Tg O_3; Atmospheric Chemistry and Climate Model Intercomparison Project, ACCMIP: 337 ± 23 Tg O_3; TOAR: 340 ± 34 Tg O_3; and Intergovernmental Panel on Climate Change, IPCC: 347 ± 28 Tg O_3 (Szopa et al., 2021). The trend in tropospheric ozone burden is within the range of trends simulated by CMIP 6 model ensemble: 0.4 to 1.3 Tg O_3/yr, as reported by Wang et al. 2022. When integrated from 60°S to 60° N, we simulate a climatological mean tropospheric ozone burden of ~287.4 Tg O_3 (lower end of the range of 287-311 Tg O_3 estimated by satellite products for 2014-2016 period; Gaudel et al. 2018), with an increasing trend of 0.68 Tg O_3/yr (close to the trend of 0.82 ± 0.13 Tg O_3/yr simulated by CMIP 6 ensemble members; Griffiths et al. 2021).

We simulate a substantial amount of tropospheric ozone attributed to stratospheric influx in the NOx-tagged (~91.5 Tg O_3 (~29 %); Table 2) and RC-tagged simulation (~76.0 Tg O_3 (~24 %); Table 4). The larger amount of ozone attributed to stratospheric influx in the NOx-tagged simulation compared to the RC-tagged simulation is because of the production of tropospheric O_3 attributed to NO_x from the stratosphere formed by the oxidation of N_2O, which is then subsequently transported into the troposphere. As described in Section 3.1.2 of Butler et al. (2018), ozone production in the stratosphere is handled directly in the chemical mechanism with the addition of new reactions producing the relevant odd oxygen species. Similarly, production of NO in the stratosphere from the oxidation of N_2O by O1D is also handled directly with an additional chemical reaction.

We attribute minor ozone production pathways with the "Extra Production" tag. In our NOx-tagged simulation this category consists of O_x production from the self-reaction of OH radicals, and from reactions between HO_2 and organic peroxy-radicals. In our RC-tagged simulation this category consists of O_x production from the self-reaction of OH radicals, and production of HO_2 from the reaction of OH with H_2O_2. The contribution of these minor production pathways to the total tropospheric ozone burden is not very substantial (up to 2 %; Table 2 and Table 4)

3.2.1 Tropospheric ozone burden attributed to NOx emission sources.

Our simulation shows that ~71 % of tropospheric ozone is attributed to NO_x emissions (both surface-based and aloft). The remaining ~29 % of tropospheric ozone burden is attributed to the stratospheric influx, and a small contribution from minor

production pathways, as discussed above. We note that the tropospheric ozone attributable to stratospheric influx in our NOx-tagged simulation is larger than the stratospheric contribution in the reactive carbon tagged simulation (24%, described below) due to the inclusion of tropospheric ozone production from stratospheric NO_x (as described above).

Anthropogenic NO_x emissions are the largest contributors to tropospheric ozone (~117 Tg O_3 (~ 37 %)), followed by lightning NO_x (~71 Tg O3 (22 %)), biogenic NO_x emissions (24 Tg O3(7.44 %)) and aircraft NO_x emissions (13.44 Tg O_3 (~4.23 %); Table 2). Lightning NO_x has a large contribution despite a small amount of NO_x emissions because of large Ozone Production Efficiency (OPE) of NO_x when emitted aloft (Table 2). Further discussion about OPE is provided in section 3.3. Biomass burning NO_x emissions contribute ~4 % to the total tropospheric ozone burden.

Among regional anthropogenic NO_x sources, the contribution from the "Rest of the World" used in this study (Table 1) to the tropospheric ozone burden is largest among the anthropogenic NO_x emissions, followed by ship NO_x emissions. This "Rest of the World" contribution is even larger than that of East Asian contribution which is the region with the largest anthropogenic NO_x emission among continental regions considered in this study (Fig. 3, Table 2). This is due to more efficient production of ozone and convection into the free troposphere at the tropical regions (Zhang et al., 2016, Zhang et al., 2021, See further discussion in section 3.3.1) that are included within the "Rest of the World" tag. The disaggregated contribution of explicitly tagged regions within the "Rest of the World" tag in our NOx-tagged simulation: Southeast Asia, Central Asia, North Africa, and Mexico-Central America (Table 1; Fig. S1b) are provided in the Supplement (Tables S5 and S6). We notice that the largest contributors among these regions are the NO_x emissions from the tropical regions: Mexico and Central America and Southeast Asia (Table S5). Similarly, the tropically situated South Asian contribution to the tropospheric ozone burden is larger than that of European contribution despite having a smaller amount of NO_x emissions (Table 2), due to the larger convection into the free troposphere as stated above.

To illustrate the predominant role of convection in transporting ozone and it's precursors at the tropics into the free troposphere, we show the zonal mean vertical profiles of annual mean O_3 and NO_x (sum of NO and NO_2) mixing ratios for the 2000-2018 climatological mean attributed to NO_x emitted from a typical tropical region: Southeast Asia and a typical northern mid-latitude region: Europe (Fig. 6; see Fig. S1 for the location of defined regions). The vertical gradient in the ozone attributed to European NO_x is consistent with summertime production of ozone primarily within the boundary layer with subsequent vertical transport into the free troposphere. While there is indeed some ozone attributed to Southeast Asian NO_x emissions present in the boundary layer, the mixing ratio of this attributed ozone is much higher in the free troposphere, which is consistent with ozone production aloft. This is due to emitted NO_x directly being transported aloft, eventually leading to free tropospheric ozone production. Further, we also note the increasing trend in NO_x burden attributed to anthropogenic NO_x emissions in the free troposphere (above 700 hPa; Figure S5)

The contribution from ship NO_x is also large due being emitted at remote ocean regions where ship NO_x is the only source of NO_x emissions. This results in less competition among tagged NO_x sources in producing ozone leading to very efficient ozone production from ship NO_x (Butler et al., 2020). Further discussion about ozone production efficiency of ship NO_x is provided in section 3.3.1.

The sign of the trend in the contribution to the tropospheric ozone burden from each of the tags (Fig. 5 (a,c)) is consistent with the sign of the NO_x emissions trend (Fig. 3 (a,c), Table 3). The percentage slope (ignoring the sign) of the trend in the contribution to tropospheric ozone burden by regional anthropogenic NO_x sources, however, is generally smaller than that of NO_x emission trend (Table 3). Similarly, the magnitude of the percentage slope in the trend in tropospheric ozone burden attributed to East Asian NO_x emissions for both the pre-2011 (2000-2011) and post-2011 (2011-2018) periods is smaller compared to the corresponding percentage slope in East Asian NO_x emissions trend (Table S2). The reason for this is due to changing ozone production efficiency with changing NO_x emissions, explained in detail in section 3.3.1.

We simulate a trend of ~0.28 Tg O_3/yr (2.41 %/yr; Table 3) in ozone burden attributed to aircraft NO_x emissions, which is comparable to 0.3 TgO_3/yr estimated by Wang et al. (2022) using sensitivity simulations, where the difference between a simulation with transient aircraft emissions and that with fixed aircraft emissions delivers the exclusive impact of changing aircraft emissions over the 1995-2017 period. While the trend derived from our tagged simulation only delivers the trend in contribution from aircraft NO_x emissions, a sensitivity simulation would also cover the changes in simulated ozone contributed from various sectors when their ozone production efficiency changes as a result of emissions being held constant. A combination of sensitivity simulations with tagging included would help us track these non-linearities and compensating feedbacks that would otherwise not be seen from sensitivity-only or tagging-only simulations.

3.2.2 Tropospheric ozone burden attributed to reactive carbon emission sources.

In our RC-tagged simulation ~76 % of the total amount of tropospheric ozone burden is attributed to tropospheric reactive carbon, while the remaining ~24 % is attributed to stratospheric influx and minor production pathways as discussed above. Of the reactive carbon sources, methane oxidation is the largest contributor to the tropospheric ozone burden (~132 Tg O_3 (42%); Table 4) and is consistent with previous studies (Young et al., 2013, Butler et al., 2018). We simulate an increasing trend with high certainty in the part of the tropospheric ozone burden attributed to RC from methane oxidation (Fig. 5b), consistent with the increasing methane oxidation rate during the 2000-2018 period as shown in Fig. 4a.

The contribution to tropospheric ozone burden from biogenic NMRC emissions (53 Tg O_3 (~17 %); Table 4) is much smaller than that of methane, despite having a comparable mass of RC emissions from both sources. This is consistent with the smaller number of oxidisable bonds per carbon atom in biogenic emissions, mainly isoprene (2.8) compared with methane (4) and the

385 subsequently lower number of NO to NO_2 conversions possible (per carbon atom) during isoprene oxidation compared with methane oxidation (Edwards and Evans, 2017). We simulate much smaller contributions of NMRC emissions from biomass burning, and aircraft NMRCs compared to biogenic and anthropogenic sources (consistent with Butler et al., 2020; Table 4). Contribution to tropospheric ozone attributed to anthropogenic NMRC emissions is relatively low at ~46 Tg O_3 (14 %; Table 4).

390

Regional anthropogenic tags each contribute less than 5 % to the total tropospheric ozone burden. The sign of the trend in tropospheric ozone attributed to most of the tags, including regional anthropogenic NMRC tags, in our RC-tagged simulation is consistent with that of the trend in the corresponding reactive carbon emissions (Table 5). We also note that the percentage trend in contribution to tropospheric ozone burden from anthropogenic NMRC (1.03 %/yr) is more than that of the trend in
395 anthropogenic NMRC emissions (0.61 %/yr), whereas the trend in contribution from methane oxidation (0.33 %/yr) is less than that of trend in methane oxidation rate (0.42 %/yr). While the biogenic NMRC emissions show an increasing trend with medium certainty, the trend in its absolute contribution to tropospheric ozone burden shows a small trend with low certainty.

3.3 Ozone production efficiency (OPE)

We estimate ozone production efficiency of emissions of any given sector as the ratio of annual mean tropospheric ozone
400 burden (in mol O_3) attributed to that sector to the amount of ozone precursors emitted in a given year (either NO_x (in mol N) or reactive carbon (in mol C)). Several previous studies report OPE as the ratio of response in tropospheric ozone burden to change in emissions introduced in the model, or as a ratio of the production rate of ozone to the loss rate of NO_x (e.g. Liu et al., 1988, Kim et al., 2016, Miyazaki et al., 2020, Archibald et al., 2020, etc.). Since our model directly calculates the ozone attributed to emissions from tagged emission sources, the ratio of the attributed tropospheric ozone burden to the emitted
405 amount of ozone precursor is calculated as OPE of that tagged precursor source. This can only be made possible when the NO_x and reactive carbon precursors are tagged in two separate simulations, as explained in Butler et al., (2020). A similar metric: Ozone Burden Efficiency (OBE) has been defined by Mertens et al., (2024), as the ratio of ozone attributed of precursor emissions (both NO_x and RC) from a given source using the combinatorial tagging approach (in Tg O3) to the emitted NO_x (Tg NO) for various tagged sectors.

410 ### 3.3.1 OPE of NO_x emissions.

Lightning NO_x (5.93 mol O_3/mol N) and aircraft NO_x (4.19 mol O_3/mol N) are most efficient at producing ozone (Fig. 6(a), Table 2) directly into the free troposphere, due to being emitted aloft (Hoor et al., 2009, Dahlmann et al., 2011). NO_x emissions aloft are highly efficient at producing ozone due to the relatively low quantities of NO_x at higher altitudes. Low NO_x concentrations increase the ozone production efficiency of NO_x due to a lower frequency of radical termination reactions
415 compared with higher NO_x concentrations, so that each molecule of NO_x can produce more molecules of ozone before being

lost by reaction with OH (Seinfeld and Pandis, 2016). In contrast, biogenic (1.4 mol O_3/mol N), biomass burning (0.88 mol O_3/mol N), and anthropogenic NO_x (0.96 mol O_3/mol N) are comparatively less efficient at producing ozone as they are emitted at the surface into regions with comparatively large NO_x concentrations.

420   Among regional anthropogenic NO_x emissions, Rest of the World is the most efficient (1.8), as it mainly consists of tropical regions where the convection into the free troposphere is large. We further elaborate the explicitly tagged regions in our NOx-tagged simulation within the Rest of the World tag in Table S7. The tropical regions: Mexico and Central America (1.81 mol O_3/mol N), and Southeast Asia (1.98 mol O_3/mol N) are the most efficient among all the explicitly tagged regions. The larger sensitivity of tropospheric ozone to emission changes in these tropical regions has also been noted in Zhang et al., (2021).

425   Similarly, OPE of South Asian NO_x (0.78 mol O_3/mol N) and to some extent Middle Eastern NO_x (0.64 mol O_3/mol N) is much larger compared to that of North American (0.54 mol O_3/mol N), European (0.36 mol O_3/mol N), Russia-Belarus-Ukraine region's (0.4 mol O_3/mol N) and East Asian (0.54 mol O_3/mol N) NO_x, for being more tropically situated (e.g., Wild et al., 2001, Butler et al., 2020, Zhang et al., 2021 etc.). International shipping is the second most efficient (1.67 mol O_3/mol N) source of anthropogenic NO_x emissions in producing ozone, due to their presence at remote pristine regions where there is a much smaller availability of other sources of NO_x (Lawrence and Crutzen 1999, Butler et al., 2020). We note that the chemistry occurring within the expanding plume emitted by ships is not considered in our coarse resolution model, leading to an instantaneous dilution of emitted NO_x into the large grid cells (Vinken et al. 2011) thereby making ozone production from Ship NO_x more efficient than observed (Kim et al. 2016).

435   The increasing trend in anthropogenic NO_x emissions from South Asia, Middle East, and international shipping (Fig. 3c and Table 3) results in less efficient production of tropospheric ozone from these sources over time (Fig. 7c and Table 3). Similarly, there is an increasing trend in OPE of anthropogenic NO_x emissions from regions with decreasing emissions (North American, European, and Russia-Belarus-Ukraine regions; Fig. 7c). The decreasing (increasing) NO_x emissions from regional anthropogenic sources becoming more (less) efficient at producing ozone, and this leads to a dampening effect where there is a smaller percentage slope (ignoring the sign) in tropospheric ozone burden compared to the slope in NO_x emissions (Table 3). This result is also consistent with Mertens et al., (2024) where an increase in NO_x emission from various tagged sectors is associated with a decrease in OBE in both present-day and future scenarios.

   Fig. 7c shows that the OPE of East Asian NOx has a trend of low certainty over the 2000-2018 period. However, when shorter periods are considered, it decreases with high certainty during the pre-2011 period when emissions increase (2000-2011 period) and increases with high certainty for the post-2011 period when emissions decrease (2011-2018 period; Table S2).

   In case of total anthropogenic NO_x emissions, we do not simulate a decrease in their OPE despite their increasing emission trend. We rather simulate an increase in OPE of anthropogenic NO_x with high certainty. This is due to an equatorward shift in

450 emissions over the 2000-2018 period (Fig. S4), where the emitted NO_x from the tropics and the subsequently formed ozone and NO_y (NO_x and reservoir species for NO_x; e.g., NO_3, N_2O_5 etc.) molecules are rapidly lifted into the free troposphere as discussed previously (Zhang et al., 2016). We also notice that the increase in anthropogenic emissions leads to a decreasing trend in OPE of other natural sources of NO_x such biogenic, biomass burning and lightning, as these natural sources must compete with more NO_x emissions from anthropogenic sources in order to produce ozone.

3.3.2 OPE of reactive carbon emissions.

Consistent with Butler et al., (2020), we simulate methane oxidation as the most efficient (0.08 mol O3/mol C; Table 4) among the tagged reactive carbon sources in our RC-tagged simulation. Similarly, we simulate smaller OPEs for biogenic (0.03 mol O3/mol C), biomass burning (0.02 mol O3/mol C), and anthropogenic (0.04 mol O3/mol C) reactive carbon sources. As noted in section 3.2.2, RC from methane oxidation is expected to be more efficient at producing ozone per unit of carbon due to the

460 higher number of oxidisable bonds per carbon atom. Anthropogenic reactive carbon emissions might be expected to be more efficient than biogenic reactive carbon emissions at producing ozone due to their proximity to anthropogenic NO_x emissions, but we see no large differences in OPE in our study (Table 4).

We simulate a trend with low certainty in the OPE RC from natural sources such as biogenic, biomass burning and methane

465 oxidation (Fig. 7; Table 5). We do simulate an increasing trend with high certainty in the OPE of global anthropogenic reactive carbon emissions. Among the regional anthropogenic sources, we simulate trends with low-medium certainty for European, South Asian and Rest of the World RC emissions. We simulate increasing trend for North American and East Asian emissions, and a decreasing trend for the OPE of the remaining tagged regional anthropogenic reactive carbon emissions. OPE of East Asian anthropogenic RC emissions have a small trend with low certainty over the 2000-2011 period and then increases with

470 high certainty during the 2011-2018 period (Table S6)

We would expect that the ozone production by reactive carbon emissions should mainly depend on the availability of NO_x, especially in pristine environments. The trends in the OPE of regional anthropogenic NMRC emissions largely, but not always, follow the trends in the emissions of NO_x in their vicinity (Table 3 and 5). However, the trends in the emission of the RC from

475 a given sector itself could influence the OPE of its own emissions, and the OPE of the NMRC emissions from other sources. For example, Butler et al., (2020) illustrate how an increase in prescribed methane concentration leads to smaller OPE of not just RC from methane oxidation but also of other tagged RC emission sectors. To better understand the behaviour of changes in OPE of reactive carbon emissions, further studies could investigate the OPE changes from perturbation simulations, by enabling ozone source attribution with tagging in the simulations. Mertens et al., (2018) demonstrate that the combination of

480 tagging and perturbation can be used to explain the compensating feedbacks induced by perturbation, from various tags used in the simulations.

3.4 Contributions from tagged precursor emission sources to surface ozone.

In this subsection, we discuss the contribution of various NO_x and reactive carbon sources to both the global surface mean and population weighted mean ozone. We further contrast this contribution with that of their contribution to the tropospheric ozone burden (discussed in section 3.2).

We select the population count for the year 2020 Gridded Population of the World (Center for International Earth Science Information Network – CIESIN – Columbia University, 2018) and scale the surface ozone according to this distribution to calculate the global population-weighted mean ozone, which is related to the ozone exposure. Choosing only one year for population weighting gives the exclusive effect of changing emissions and not the effect of changing population. Future studies may consider scaling according to a transient population over the analysis period rather than fixing it at one year (year 2020 in this study). Table S9 provides the population, and their fraction of world population (in %), for the regions considered in this study.

We simulate ~ 25.4 ppbv of global mean surface ozone with an increasing trend of high certainty (0.08 ppbv/yr (0.3 %/yr); Fig. 7 and Table 3). Similarly, we simulate ~33.0 ppbv of global population-weighted mean ozone with an increasing trend and slightly larger slope (0.17 ppbv/yr (0.54 %/yr); Fig. 8 and Table 3) compared to global surface mean ozone. We will explain the main contributors responsible for this increasing trend and the larger slope in global mean population-weighted ozone in the subsequent discussion. DeLang et al., 2021 showed that the increasing trend in global ozone exposure is mainly driven by increasing ozone exposure at highly populated regions such as Asia and Africa. In our study, we quantify the contribution of various ozone precursor emission sources to the global population-weighted surface ozone and its trend.

The share of the stratospheric contribution to the global mean surface ozone (4-5 ppbv (~15-20%); Table 2 and Table 4), is smaller than its contribution to tropospheric ozone burden (24-29 %; Table 2 and Table 4). We simulate an increasing trend with high certainty (~ 0.3-0.4 %/yr; Table 3 and Table 5) in this contribution mainly over the southern hemisphere (not shown). The stratospheric contribution to the population weighted surface ozone is much smaller (~3 ppbv (9-11 %); Table 2 and Table 4) compared to the quantities discussed above, as this is mainly contributing over remote regions such as polar and oceanic regions (not shown).

3.4.1 Surface ozone attributed to NO_x emissions.

The percentage contribution to global mean surface ozone from sources aloft (lightning, aircraft, stratosphere) is smaller compared to the contribution to tropospheric ozone burden (Table 2). Consequently, the surface-based NO_x sources (biogenic,

biomass burning and anthropogenic) contribute a larger share to the global mean surface ozone compared to their share of the tropospheric ozone burden.

515 The share of the anthropogenic NO_x contribution has the largest difference in its contribution from ~37 % (to tropospheric ozone burden) to ~48 % (to global mean surface ozone; Table 2). All the tagged regional anthropogenic NO_x sources contribute a larger percentage share to global mean surface ozone than to the tropospheric ozone burden (Table 2). However, the tropically situated explicitly tagged regions within the "Rest of the Word" tag in our NOx-tagged simulation: Mexico and Central America, and Southeast Asia have smaller share in their contribution to global mean surface ozone compared to that of

520 tropospheric ozone burden (Table S7), largely due to being situated in a tropical region with large convection to the free troposphere (Fig 6; Zhang et al., 2016; Zhang et al., 2021). We simulate a small increasing trend (0.08 ppbv/yr (0.30 %/yr); Table 3) in global mean surface ozone, mainly driven by increasing stratospheric contribution (0.02 ppbv/yr (~0.32 %/yr)) and increasing trend in contribution from anthropogenic NO_x sources (0.08 ppbv/yr (0.69 %/yr); Table 3 and Fig 7c).

525 The contribution from anthropogenic NO_x to the population weighted surface ozone (~20 ppbv (62 %;) Table 2) is larger than its contribution to global mean surface ozone. This larger contribution is compensated by smaller remote contributions such as stratosphere, lightning, aircraft, and biomass burning. Among the regional anthropogenic sources, the NO_x emissions from highly populated regions (see Table S9 for population of world regions): South Asia (4.6 ppbv (~14 %),) East Asia (~4.3 ppbv (13 %)) and Rest of the World (~4.3 ppbv (13 %)) are the largest contributors to global population-weighted mean ozone. Ship

530 NO_x emissions also have a substantial contribution (~2.5 ppbv (7.5 %)) to the global population-weighted surface mean ozone, larger than contributions from anthropogenic NO_x emissions by relatively sparsely populated world regions such as North America, Europe, Russia-Belarus-Ukraine region, or Middle East (Table 2). The increasing trend in global population-weighted surface ozone (0.17 ppbv/yr (0.54%/yr); Table 3) which is slightly larger compared to the trend in global mean surface ozone, is mainly driven by increasing anthropogenic NO_x emissions especially from highly populated regions (South

535 Asia, East Asia and "Rest of the World") and from international shipping. Despite NOx emissions from international shipping happening only over ocean grid cells, the ozone attributed to ship NOx spreads across land areas and contributes to the total surface ozone by ~3-6 ppb (Fig. 10a). Although there is no population over the regions where international ship NO_x is emitted, the global population weighted mean ozone attributed to ship NOx is comparable to that of global mean surface ozone (Table 2) as large populations at several coastal areas and densely populated inland regions in East Asia and South Asia are exposed

540 to ozone attributed to ship NOx emissions (Fig. 10b). We notice that while there is a steep decreasing slope after year 2013 in global mean surface ozone attributed to East Asian NO_x emissions (Fig. 8c; due to emission reduction shown in Fig. 3c), we do not find a similar feature for global population-weighted mean ozone attributed to East Asian NO_x emissions (Fig. 9c and Table S2). The reason for this is unclear at this point and could be an interesting topic for future studies.

3.4.2 Surface ozone attributed to reactive carbon emissions.

545 RC from methane oxidation contributes ~12 ppbv (47 %) to global mean surface ozone, biogenic and anthropogenic NMRC emissions contribute ~4.1 ppbv (~16 %) and 3.72 ppbv (~14.7 %; Table 4) respectively. Regional anthropogenic tags each contribute less than 5 % to the global mean surface ozone. Since the percentage contribution from stratospheric influx on global mean surface ozone is smaller than it's contribution to tropospheric ozone burden (as explained above), there is larger contribution from methane oxidation, anthropogenic and biomass burning RC emissions. We simulate a small trend with low

550 certainty in the contribution to global mean surface ozone from anthropogenic NMRC emissions (Table 5). The increasing trend in global mean surface ozone is mainly driven by increasing contribution from stratosphere, RC from methane oxidation, and biogenic NMRC emissions. Although there is no trend with high certainty in emissions of biogenic NMRC, its increasing contribution to global mean surface ozone (Table 5) could be explained by the increasing anthropogenic NO_x emissions (Butler et al., 2018, Lupascu et al., 2022).

555

The largest contribution to global population-weighted mean surface ozone is from ozone attributed to RC from methane oxidation (~12 ppbv (37 %); Table 4). This Contribution is smaller compared to its contribution to global mean surface ozone (~47 %), because a substantial part of this contribution to global mean surface ozone is at remote oceanic regions (not shown).

560 Consequently, there is a larger relative contribution from biogenic (22 %) and anthropogenic (25%) NMRC sources to global population weighted mean ozone compared to their contribution to global mean surface ozone. Among regional anthropogenic NMRC emissions, there is a larger share of contributions from highly populated regions such as South Asian, East Asian and Rest of the World, and a smaller share from North American, European, and Russia-Belarus-Ukraine region's anthropogenic NMRC emissions to global population-weighted mean ozone compared to contribution to global mean surface ozone (Table

565 4).

The increasing trend in population-weighted surface ozone is mainly driven by increasing trends in the contribution of RC from methane oxidation (0.05 ppbv/yr (0.38 %/yr)), anthropogenic (0.09 ppbv/yr (1.23 %/yr)) and biogenic (0.03 ppbv/yr (0.44 %/yr)) NMRC emissions (Table 5). McDuffie et al. (2023) show that with a ~100 ppb of methane pulse, the population-

570 weighted ozone response is larger than the response in the global mean surface ozone. They further explain that this larger response was due to the larger availability of NO_x precursor emissions at populated regions leading to larger ozone production in populated regions. In contrast, we simulate a larger trend in contribution from methane oxidation to global mean (0.42 %/year) than to population-weighted mean surface ozone (0.38 %/year; Table 5), despite having a comparable change in prescribed methane concentration (~135 ppb; Fig. 4) over the 2000-2018 period. This is due to a dominant trend in contribution

575 from anthropogenic NMRC emissions from populated regions in our simulation, which is lacking in the methane pulse simulated by McDuffie et al. (2023). This dominant trend in anthropogenic NMRC contribution to population-weighted surface

ozone can also be seen in its significantly increasing relative contribution (Figure S8), which is not seen in other major contributors such as methane and biogenic NMRCs.

580 The total NO_x emissions show a positive trend leading to increasing contribution from methane oxidation. Similarly, the increasing anthropogenic NO_x emitted at densely populated regions reacts with NMRC emitted from anthropogenic and biogenic sources (Fig. 8b; Lupascu et al., 2022). Among regional anthropogenic NMRC emissions, the contribution from highly populated regions (Table S9): South Asia (~0.07 ppbv/yr (3.61 %/yr)) and East Asia (~0.06 ppbv/yr (2.85 %/yr); Table 4) to global population-weighted ozone shows the largest increasing trend. As for the NOx-tagged case discussed in the previous subsection, the global population-weighted ozone attributed to East Asian anthropogenic NMRC emissions shows a small trend with low certainty during the post-2011 period in response to the reduction in emissions (Table S6).

4 Summary and Conclusions

In this study we quantify the contributions of ozone precursor emissions from various sources to tropospheric ozone during the 2000-2018 period. For this, we use the tagging approach using CAM4-Chem introduced in Butler et al., 2018. We perform separate simulations for NO_x and RC-tagged contributors to tropospheric ozone which allows us to quantify the absolute contribution from the tagged emission sources to the tropospheric ozone burden and calculate the ozone production efficiency per tagged sector/region.

We note a decreasing trend in both anthropogenic NO_x and reactive carbon ozone precursor emissions from North America, Europe, and Russia-Belarus-Ukraine region, and increasing trend from East Asia, South Asia, Middle East, international shipping, and Rest of the World. We simulate the largest contribution to tropospheric ozone burden from anthropogenic NO_x emissions (in our NOx-tagged simulation) and reactive carbon from methane oxidation (in our RC-tagged simulation), both with significantly increasing trend, followed by contribution of ozone influx from stratosphere but with no significant trend in its contribution. We simulate a relatively larger contribution to the tropospheric ozone burden from emissions at tropical regions compared to other regions, as previously discussed in Zhang et al., (2021). For example, the anthropogenic NO_x emissions from "rest of the world" regional tag that mainly consists of tropical and southern hemisphere regions, contributes more to the tropospheric ozone burden compared with East Asia despite smaller NO_x emissions. We show using vertical profiles of tagged O_3 and NO_x mixing ratio fields (Fig. 6) that it is the emitted NO_x in the tropics which predominantly gets lofted into the free troposphere and eventually form ozone. Our tagging method only conveys information on the precursor source of the simulated ozone and associated gas molecules. It, however, does not convey information about where exactly the ozone molecule was formed: in the free troposphere, or within the boundary layer. While addressing this is beyond the scope of our study, further studies could employ ozone tagging method used in Sudo and Akimoto (2007) and Derwent et al., (2015)

that tag/label ozone molecules based on the location at which the ozone molecules are formed. Our study highlights the dominant effect of equatorward shifting of O_3 precursor emissions which contributes to the tropospheric O_3 burden trend. Nevertheless, there remain other climatic factors that may play an amplifying or offsetting role to these contributions. These include, for example, changes in the general circulation of the atmosphere and monsoonal changes under a warming planet, as well as the natural variability of climate.

The trend in each tagged sectors' contribution to the total tropospheric ozone burden is consistent with the sign of trend in the respective precursor emission from that tagged sector. We simulate an increasing trend in OPE of NO_x emissions from regions where the emissions are decreasing (European, North American, and Russia-Belarus-Ukraine region's emissions) and vice versa (South Asian and Middle East). The anthropogenic NMRC becomes more efficient at producing ozone, following the increasing trend in anthropogenic NO_x emissions in their vicinity. We, however, do not simulate any trends with medium-high certainty in the OPE of other major reactive carbon sources such as methane oxidation, biogenic and biomass burning. We therefore recommend that further studies perform simulations combining perturbation and tagging to investigate how perturbation in the emissions of one sector induces changes in OPE of itself and other tagged sectors.

We contrast the contribution of emissions from tagged sectors to the global tropospheric ozone burden with their contribution to the global mean surface ozone and the population weighted mean surface ozone. Except for tropical source regions such as South Asia, we simulate a larger share of contributions from regional anthropogenic NO_x emissions to the global mean surface ozone compared to the tropospheric ozone burden. We also simulate an increasing trend in contribution by RC from methane oxidation and biogenic NMRC to global mean surface ozone and population-weighted mean ozone, leading to an overall global increasing trend in both these quantities. The increasing trend in population weighted ozone is mainly driven by increasing trend in contribution from anthropogenic NO_x and (to a lesser extent) NMRC emissions over highly populated regions: South Asia and East Asia. We also simulate a substantial contribution of NO_x emissions from international shipping to the population weighted mean ozone. While the focus of the present study has been the quantification of the influences on global ozone metrics, future work using the methods employed in this study could focus on quantification of the intra- and extra-regional contributions to surface ozone in the regions studied here.

In our study, we discuss the results related to the 2000-2018 trends in global annual ozone metrics and its precursor emissions. Further studies could investigate the tagged contributions to the trends in the spatial and seasonal distribution of ozone (e.g., Wang et al. 2022, Fiore et al., 2022), which may help us enhance our understanding of various processes responsible for these trends. While previous studies used the TOAST tagging to understand the trends in surface ozone over United States (e.g., Li et al., 2023a), free tropospheric ozone over Southeast Asia (e.g., Li et al., 2023b) and over East Asia in future scenarios (e.g., Hou et al., 2023), we recommend such studies be extended to other regions of interest. Comparison of smaller time periods (2000-2011, and 2011-2018) could also be considered to understand the contrasting effect of increasing and decreasing East

Asian precursor emissions respectively. Finally, we recommend other global models implement the tropospheric ozone source attribution with NO_x and RC tagging separately, which would enable a more rigorous model intercomparison and a better understanding of the underlying processes leading to the inter-model spread in their estimation of tropospheric ozone.

645

Acknowledgements

The authors would like to thank Mark Lawrence, Louisa Emmons, Claire Granier, Jukka-Pekka Jalkanen, Jan Eiof Jonson and Mariano Mertens for their helpful discussions during the performance of our simulations and preparation of this paper. Simulations were performed on the high-performance supercomputing cluster GLIC at the GFZ, Potsdam.

650 **Financial support**

This research has been supported by the Bundesministerium für Bildung und Forschung (grant no. 01US1701).

Data Availability

The values in the timeseries plotted in this study (Figures 3, 5, 7, 8, and 9) are provided in the Supplementary material. Please contact tim.butler@rifs-potsdam.de for availing the model output of our simulations.

655 **Supplementary materials**

Attached documents are: noxtagged_annual.csv, rctagged_annual.csv, Supplementary-figures-tables.docx

Author Contributions

AN designed the study and model simulations with support from AL and TB. TA has performed the simulations with support from AN, AL and TB. AN has written the paper with inputs from AL, TB and TA. TA supported with population-weighted
660 ozone analysis.

Competing Interests

At least one of the (co-)authors is a member of the editorial board of Atmospheric Chemistry and Physics

References

665 Archibald, A., Neu, J., Elshorbany, Y., Cooper, O., Young, P., Akiyoshi, H., Cox, R., Coyle, M., Derwent, R., Deushi, M., et al.: Tropospheric Ozone Assessment Report: A critical review of changes in the tropospheric ozone burden and budget from 1850 to 2100, Elem Sci Anth, 8, 034, 2020.

Avnery, S., Mauzerall, D. L., Liu, J., and Horowitz, L. W.: Global crop yield reductions due to surface ozone exposure: 1. Year 2000 crop production losses and economic damage, Atmospheric Environment, 45, 2284–2296, 2011.

670

Bak, J., Song, E.-J., Lee, H.-J., Liu, X., Koo, J.-H., Kim, J., Jeon, W., Kim, J.-H., and Kim, C.-H.: Temporal variability of tropospheric ozone and ozone profiles in the Korean Peninsula during the East Asian summer monsoon: insights from multiple measurements and reanalysis datasets, Atmospheric Chemistry and Physics, 22, 14 177–14 187, 2022.

Butler, T. J., Vermeylen, F. M., Rury, M., Likens, G. E., Lee, B., Bowker, G. E., and McCluney, L.: Response of ozone and 675 nitrate to stationary source NOx emission reductions in the eastern USA, Atmospheric Environment, 45, 1084–1094, 2011.

Butler, T., Lupascu, A., and Nalam, A.: Attribution of ground-level ozone to anthropogenic and natural sources of nitrogen oxides and reactive carbon in a global chemical transport model, Atmospheric Chemistry and Physics, 20, 10 707–10 731, 2020.

Butler, T., Lupascu, A., Coates, J., and Zhu, S.: TOAST 1.0: Tropospheric ozone attribution of sources with tagging for CESM 680 1.2. 2, Geoscientific Model Development, 11, 2825–2840, 2018.

Center for International Earth Science Information Network - CIESIN - Columbia University. 2018. Gridded Population of the World, Version 4 (GPWv4): Population Count. Palisades, NY: NASA Socioeconomic Data and Applications Center (SEDAC). http://dx.doi.org/10.7927/H4X63JVC

Chameides, W. and Walker, J. C.: A photochemical theory of tropospheric ozone, Journal of Geophysical Research, 78, 8751– 685 8760, 1973.

Chang, K.-L., Schultz, M. G., Koren, G., and Selke, N.: Guidance note on best statistical practices for TOAR analyses, arXiv preprint. arXiv:2304.14236, 2023.

Chua, G., Naik, V., and Horowitz, L. W.: Exploring the drivers of tropospheric hydroxyl radical trends in the Geophysical Fluid Dynamics Laboratory AM4.1 atmospheric chemistry–climate model, Atmos. Chem. Phys., 23, 4955–4975, https://doi.org/10.5194/acp-23-4955-2023, 2023.

Coates, J. and Butler, T. M.: A comparison of chemical mechanisms using tagged ozone production potential (TOPP) analysis, Atmospheric Chemistry and Physics, 15, 8795–8808, 2015.

Cooper, O. R., Parrish, D., Ziemke, J., Balashov, N., Cupeiro, M., Galbally, I., Gilge, S., Horowitz, L., Jensen, N., Lamarque, J.-F., et al.: Global distribution and trends of tropospheric ozone: An observation-based review, Elementa, 2, 000 029, 2014.

Crippa, M., Guizzardi, D., Butler, T., Keating, T., Wu, R., Kaminski, J., Kuenen, J., Kurokawa, J., Chatani, S., Morikawa, T., et al.: HTAP_v3 emission mosaic: a global effort to tackle air quality issues by quantifying global anthropogenic air pollutant sources, Earth System Science Data Discussions, 2023, 1–34, 2023.

Crutzen, P. J.: Photochemical reactions initiated by and influencing ozone in unpolluted tropospheric air, Tellus, 26, 47–57, 1974.

Dahlmann, K., Grewe, V., Ponater, M., and Matthes, S.: Quantifying the contributions of individual NOx sources to the trend in ozone radiative forcing, Atmospheric Environment, 45, 2860–2868, 2011.

DeLang, M. N., Becker, J. S., Chang, K.-L., Serre, M. L., Cooper, O. R., Schultz, M. G., Schröder, S., Lu, X., Zhang, L., Deushi, M., et al.: Mapping yearly fine resolution global surface ozone through the Bayesian maximum entropy data fusion of observations and model output for 1990–2017, Environmental science & technology, 55, 4389–4398, 2021.

Derwent, R. G., Utembe, S. R., Jenkin, M. E., and Shallcross, D. E.: Tropospheric ozone production regions and the intercontinental origins of surface ozone over Europe, Atmospheric Environment, 112, 216–224, 2015.

Edwards, P. M. and Evans, M. J.: A new diagnostic for tropospheric ozone production, Atmospheric Chemistry and Physics, 17, 13 669–13 680, 2017.

Emmons, L. K., Schwantes, R. H., Orlando, J. J., Tyndall, G., Kinnison, D., Lamarque, J.-F., Marsh, D., Mills, M. J., Tilmes, S., Bardeen, C., et al.: The chemistry mechanism in the community earth system model version 2 (CESM2), Journal of Advances in Modeling Earth Systems, 12, e2019MS001 882, 2020.

Emmons, L., Hess, P., Lamarque, J.-F., and Pfister, G.: Tagged ozone mechanism for MOZART-4, CAM-chem and other chemical transport models, Geoscientific Model Development, 5, 1531–1542, 2012.

Fiore, A. M., Dentener, F., Wild, O., Cuvelier, C., Schultz, M., Hess, P., Textor, C., Schulz, M., Doherty, R., Horowitz, L., et al.: Multimodel estimates of intercontinental source-receptor relationships for ozone pollution, Journal of Geophysical Research: Atmospheres, 114, 2009.

Fiore, A. M., Hancock, S. E., Lamarque, J.-F., Correa, G. P., Chang, K.-L., Ru, M., Cooper, O., Gaudel, A., Polvani, L. M., Sauvage, B., et al.: Understanding recent tropospheric ozone trends in the context of large internal variability: a new perspective from chemistry-climate model ensembles, Environmental Research: Climate, 1, 025 008, 2022.

Galmarini, S., Koffi, B., Solazzo, E., Keating, T., Hogrefe, C., Schulz, M., Benedictow, A., Griesfeller, J. J., Janssens-Maenhout, G., Carmichael, G., et al.: Coordination and harmonization of the multi-scale, multi-model activities HTAP2, AQMEII3, and MICS-Asia3: simulations, emission inventories, boundary conditions, and model output formats, Atmospheric Chemistry and Physics, 17, 1543–1555, 2017.

Gaudel, A., Cooper, O. R., Ancellet, G., Barret, B., Boynard, A., Burrows, J. P., Clerbaux, C., Coheur, P.-F., Cuesta, J., Cuevas, E., et al.: Tropospheric Ozone Assessment Report: Present-day distribution and trends of tropospheric ozone relevant to climate and global atmospheric chemistry model evaluation, Elem Sci Anth, 6, 39, 2018.

Gaudel, A., Cooper, O. R., Chang, K.-L., Bourgeois, I., Ziemke, J. R., Strode, S. A., Oman, L. D., Sellitto, P., Nédélec, P., Blot, R., et al.: Aircraft observations since the 1990s reveal increases of tropospheric ozone at multiple locations across the Northern Hemisphere, Science Advances, 6, eaba8272, 2020.

Granier, C., Bessagnet, B., Bond, T., D'Angiola, A., Denier van der Gon, H., Frost, G. J., Heil, A., Kaiser, J. W., Kinne, S., Klimont, Z., et al.: Evolution of anthropogenic and biomass burning emissions of air pollutants at global and regional scales during the 1980–2010 period, Climatic change, 109, 163–190, 2011.

Grewe, V., Tsati, E., and Hoor, P.: On the attribution of contributions of atmospheric trace gases to emissions in atmospheric model applications, Geoscientific Model Development, 3, 487–499, 2010.

Grewe, V., Tsati, E., Mertens, M., Frömming, C., and Jöckel, P.: Contribution of emissions to concentrations: The TAGGING 1.0 submodel based on the Modular Earth Submodel System (MESSy 2.52), Geoscientific Model Development, 10, 2615–2633, 2017.

Griffiths, P. T., Murray, L. T., Zeng, G., Shin, Y. M., Abraham, N. L., Archibald, A. T., Deushi, M., Emmons, L. K., Galbally, I. E., Hassler, B., et al.: Tropospheric ozone in CMIP6 simulations, Atmospheric Chemistry and Physics, 21, 4187–4218, 2021.

Heald, C. L. and Kroll, J.: The fuel of atmospheric chemistry: Toward a complete description of reactive organic carbon, Science Advances, 6, eaay8967, 2020.

Hoor, P., Borken-Kleefeld, J., Caro, D., Dessens, O., Endresen, O., Gauss, M., Grewe, V., Hauglustaine, D., Isaksen, I. S., Jöckel, P., et al.: The impact of traffic emissions on atmospheric ozone and OH: results from QUANTIFY, Atmospheric Chemistry and Physics, 9, 3113–3136, 2009.

Hou, X., Wild, O., Zhu, B., and Lee, J.: Future tropospheric ozone budget and distribution over east Asia under a net-zero scenario, Atmospheric Chemistry and Physics, 23, 15 395–15 411, 2023.

Hussain, M. and Mahmud, I.: pyMannKendall: a python package for non-parametric Mann Kendall family of trend tests., Journal of Open Source Software, 4, 1556, https://doi.org/10.21105/joss.01556, 2019.

Jonson, J. E., Schulz, M., Emmons, L., Flemming, J., Henze, D., Sudo, K., Tronstad Lund, M., Lin, M., Benedictow, A., Koffi, B., et al.: The effects of intercontinental emission sources on European air pollution levels, Atmospheric Chemistry and Physics, 18, 13 655–13 672, 2018.

Junge, C. E.: Global ozone budget and exchange between stratosphere and troposphere, Tellus, 14, 363–377, 1962.
Kim, H. S., Kim, Y. H., Han, K. M., Kim, J., and Song, C. H.: Ozone production efficiency of a ship-plume: ITCT 2K2 case study, Chemosphere, 143, 17–23, 2016.

Kwok, R., Baker, K., Napelenok, S., and Tonnesen, G.: Photochemical grid model implementation and application of VOC, NOx, and O3 source apportionment, Geoscientific Model Development, 8, 99–114, 2015.

Lamarque, J.-F., Emmons, L., Hess, P., Kinnison, D. E., Tilmes, S., Vitt, F., Heald, C., Holland, E. A., Lauritzen, P., Neu, J., et al.: CAM-chem: Description and evaluation of interactive atmospheric chemistry in the Community Earth System Model, Geoscientific Model Development, 5, 369–411, 2012.

Lan, X., K.W. Thoning, and E.J. Dlugokencky: Trends in globally-averaged CH4, N2O, and SF6 determined from NOAA Global Monitoring Laboratory measurements. Version 2024-01, https://doi.org/10.15138/P8XG-AA10, 2024.

Lawrence, M. G. and Crutzen, P. J.: Influence of NOx emissions from ships on tropospheric photochemistry and climate, Nature, 402, 167–170, 1999.

Lawrence, M., Jöckel, P., and Von Kuhlmann, R.: What does the global mean OH concentration tell us?, Atmospheric Chemistry and Physics, 1, 37–49, 2001.

Lelieveld, J. a., Butler, T., Crowley, J., Dillon, T., Fischer, H., Ganzeveld, L., Harder, H., Lawrence, M., Martinez, M., Taraborrelli, D., et al.: Atmospheric oxidation capacity sustained by a tropical forest, Nature, 452, 737–740, 2008.

770 Levy II, H.: Photochemistry of the lower troposphere, Planetary and Space Science, 20, 919–935, 1972.

Li, P., Yang, Y., Wang, H., Li, S., Li, K., Wang, P., Li, B., and Liao, H.: Source attribution of near-surface ozone trends in the United States during 1995–2019, Atmospheric Chemistry and Physics, 23, 5403–5417, 2023a.

Li, S., Yang, Y., Wang, H., Li, P., Li, K., Ren, L., Wang, P., Li, B., Mao, Y., and Liao, H.: Rapid increase in tropospheric ozone over Southeast Asia attributed to changes in precursor emission source regions and sectors, Atmospheric Environment, 775 304, 119 776, 2023b.

Lin, X., Trainer, M., and Liu, S.: On the nonlinearity of the tropospheric ozone production, Journal of Geophysical Research: Atmospheres,93, 15 879–15 888, 1988.
Liu, Z., Doherty, R. M., Wild, O., O'connor, F. M., and Turnock, S. T.: Tropospheric ozone changes and ozone sensitivity from the present day to the future under shared socio-economic pathways, Atmospheric Chemistry and Physics, 22, 1209–780 1227, 2022.

Li, M., Kurokawa, J., Zhang, Q., Woo, J.-H., Morikawa, T., Chatani, S., Lu, Z., Song, Y., Geng, G., Hu, H., Kim, J., Cooper, O. R., and McDonald, B. C.: MIXv2: a long-term mosaic emission inventory for Asia (2010–2017), Atmos. Chem. Phys., 24, 3925–3952, https://doi.org/10.5194/acp-24-3925-2024, 2024.

785 Lupascu, A. and Butler, T.: Source attribution of European surface O3 using a tagged O3 mechanism, Atmospheric Chemistry and Physics, 19, 14 535–14 558, 2019.

Lupascu, A., Otero, N., Minkos, A., and Butler, T.: Attribution of surface ozone to NO x and volatile organic compound sources during two different high ozone events, Atmospheric chemistry and physics, 22, 11 675–11 699, 2022.

Malashock, D. A., DeLang, M. N., Becker, J. S., Serre, M. L., West, J. J., Chang, K.-L., Cooper, O. R., and Anenberg, S. C.: 790 Estimates of ozone concentrations and attributable mortality in urban, peri-urban and rural areas worldwide in 2019, Environmental Research Letters, 17, 054 023, 2022.

McDuffie, E. E., Sarofim, M. C., Raich, W., Jackson, M., Roman, H., Seltzer, K., Henderson, B. H., Shindell, D. T., Collins, M., Anderton,J., et al.: The Social Cost of Ozone-Related Mortality Impacts From Methane Emissions, Earth's future, 11, e2023EF003 853, 2023.

Mertens, M., Grewe, V., Rieger, V. S., and Jöckel, P.: Revisiting the contribution of land transport and shipping emissions to tropospheric ozone, Atmospheric Chemistry and Physics, 18, 5567–5588, 2018.

Mertens, M., Kerkweg, A., Grewe, V., Jöckel, P., and Sausen, R.: Attributing ozone and its precursors to land transport emissions in Europe and Germany, Atmospheric Chemistry and Physics (ACP), pp. 7843–7873, 2020.

Mertens, M., Brinkop, S., Graf, P., Grewe, V., Hendricks, J., Jöckel, P., Lanteri, A., Matthes, S., Rieger, V. S., Righi, M., and Thor, R. N.: The contribution of transport emissions to ozone mixing ratios and methane lifetime in 2015 and 2050 in the Shared Socioeconomic Pathways (SSPs), Atmos. Chem. Phys., 24, 12079–12106, https://doi.org/10.5194/acp-24-12079-2024, 2024.

Mills, G., Pleijel, H., Malley, C. S., Sinha, B., Cooper, O. R., Schultz, M. G., Neufeld, H. S., Simpson, D., Sharps, K., Feng, Z., et al.: Tropospheric Ozone Assessment Report: Present-day tropospheric ozone distribution and trends relevant to vegetation, Elem Sci Anth, 6, 47, 2018.

Miyazaki, K., Bowman, K., Sekiya, T., Takigawa, M., Neu, J. L., Sudo, K., Osterman, G., and Eskes, H.: Global tropospheric ozone responses to reduced NO x emissions linked to the COVID-19 worldwide lockdowns, Science Advances, 7, eabf7460, 2021.

Molod, A., Takacs, L., Suarez, M., and Bacmeister, J.: Development of the GEOS-5 atmospheric general circulation model: Evolution from MERRA to MERRA2, Geoscientific Model Development, 8, 1339–1356, 2015.

Monks, P. S., Archibald, A., Colette, A., Cooper, O., Coyle, M., Derwent, R., Fowler, D., Granier, C., Law, K. S., Mills, G., et al.: Tropospheric ozone and its precursors from the urban to the global scale from air quality to short-lived climate forcer, Atmospheric chemistry and physics, 15, 8889–8973, 2015.

Myhre, G., D. Shindell, F.-M. Bréon, W. Collins, J. Fuglestvedt, J. Huang, D. Koch, J.-F. Lamarque, D. Lee, B. Mendoza, T. Nakajima, A. Robock, G. Stephens, T. Takemura and H. Zhang: Anthropogenic and Natural Radiative Forcing. In: Climate Change 2013: The Physical Science Basis. Contribution of Working Group I to the Fifth Assessment Report of the Intergovernmental Panel on Climate Change [Stocker, T.F., D. Qin, G.-K. Plattner, M. Tignor, S.K. Allen, J. Boschung, A. Nauels, Y. Xia, V. Bex and P.M. Midgley (eds.)]. Cambridge University Press, Cambridge, United Kingdom and New York, NY, USA, 2021.

Prather, M. J.: Time scales in atmospheric chemistry: Theory, GWPs for CH4 and CO, and runaway growth, Geophysical Research Letters, 23, 2597–2600, 1996.

Schneider, P. and Van Der A, R.: A global single-sensor analysis of 2002–2011 tropospheric nitrogen dioxide trends observed from space, Journal of Geophysical Research: Atmospheres, 117, 2012.

825 Schultz, M. G., Schröder, S., Lyapina, O., Cooper, O. R., Galbally, I., Petropavlovskikh, I., Von Schneidemesser, E., Tanimoto, H., Elshorbany, Y., Naja, M., et al.: Tropospheric Ozone Assessment Report: Database and metrics data of global surface ozone observations, Elem Sci Anth, 5, 58, 2017.

Seinfeld, J. H. and Pandis, S. N.: Atmospheric chemistry and physics: from air pollution to climate change, John Wiley & Sons, 2016.

Sindelarova, K., Markova, J., Simpson, D., Huszar, P., Karlicky, J., Darras, S., Granier, C.: Copernicus Atmosphere 830 Monitoring Service Global Biogenic VOC emissions version 3.0 (CAMS-GLOB-BIO v3.0), ECCAD, https://doi.org/10.24380/xs64-gj42, 2021.

Sudo, K. and Akimoto, H.: Global source attribution of tropospheric ozone: Long-range transport from various source regions, Journal of Geophysical Research: Atmospheres, 112, 2007.

835 Szopa, S., V. Naik, B. Adhikary, P. Artaxo, T. Berntsen, W.D. Collins, S. Fuzzi, L. Gallardo, A. Kiendler-Scharr, Z. Klimont, H. Liao, N. Unger, and P. Zanis, 2021: Short-Lived Climate Forcers. In Climate Change: The Physical Science Basis. Contribution of Working Group I to the Sixth Assessment Report of the Intergovernmental Panel on Climate Change [Masson-Delmotte, V., P. Zhai, A. Pirani, S.L. Connors, C. Péan, S. Berger, N. Caud, Y. Chen, L. Goldfarb, M.I. Gomis, M. Huang, K. Leitzell, E. Lonnoy, J.B.R. Matthews, T.K. Maycock, T. Waterfield, O. Yelekçi, R. Yu, and B. Zhou (eds.)]. Cambridge 840 University Press, Cambridge, United Kingdom and New York, NY, USA, pp. 817–922, doi:10.1017/9781009157896.008, 2021.

Taylor, K. E.: Summarizing multiple aspects of model performance in a single diagram, Journal of geophysical research: atmospheres, 106, 7183–7192, 2001.

Tilmes, S., Lamarque, J.-F., Emmons, L., Conley, A., Schultz, M., Saunois, M., Thouret, V., Thompson, A., Oltmans, S., 845 Johnson, B., et al.: Ozonesonde climatology between 1995 and 2011: description, evaluation and applications, Atmospheric Chemistry and Physics, 12, 7475–7497, 2012.

Tilmes, S., Lamarque, J.-F., Emmons, L., Kinnison, D., Ma, P.-L., Liu, X., Ghan, S., Bardeen, C., Arnold, S., Deeter, M., et al.: Description and evaluation of tropospheric chemistry and aerosols in the Community Earth System Model (CESM1. 2), Geoscientific Model Development, 8, 1395–1426, 2015.

850   Van der Werf, G. R., Randerson, J. T., Giglio, L., Collatz, G., Mu, M., Kasibhatla, P. S., Morton, D. C., DeFries, R., Jin, Y. v., and van Leeuwen, T. T.: Global fire emissions and the contribution of deforestation, savanna, forest, agricultural, and peat fires (1997–2009), Atmospheric chemistry and physics, 10, 11 707–11 735, 2010.

Vinken, G. C., Boersma, K. F., Jacob, D. J., and Meijer, E. W.: Accounting for non-linear chemistry of ship plumes in the GEOS-Chem global chemistry transport model, Atmospheric Chemistry and Physics, 11, 11 707–11 722, 2011.

855

Voulgarakis, A., Naik, V., Lamarque, J.-F., Shindell, D. T., Young, P., Prather, M. J., Wild, O., Field, R., Bergmann, D., Cameron-Smith, P., et al.: Analysis of present day and future OH and methane lifetime in the ACCMIP simulations, Atmospheric Chemistry and Physics, 13, 2563–2587, 2013.

Wang, W., Parrish, D. D., Wang, S., Bao, F., Ni, R., Li, X., Yang, S., Wang, H., Cheng, Y., and Su, H.: Long-term trend of
860   ozone pollution in China during 2014–2020: Distinct seasonal and spatial characteristics and ozone sensitivity, Atmospheric Chemistry and Physics, 22, 8935–8949, 2022.

West, J. J., Fiore, A. M., Naik, V., Horowitz, L. W., Schwarzkopf, M. D., and Mauzerall, D. L.: Ozone air quality and radiative forcing consequences of changes in ozone precursor emissions, Geophysical Research Letters, 34, 2007.

Wild, O., Prather, M. J., and Akimoto, H.: Indirect long-term global radiative cooling from NOx emissions, Geophysical
865   Research Letters, 28, 1719–1722, 2001.

Young, P. J., Naik, V., Fiore, A. M., Gaudel, A., Guo, J., Lin, M., Neu, J., Parrish, D., Rieder, H., Schnell, J., et al.: Tropospheric Ozone Assessment Report: Assessment of global-scale model performance for global and regional ozone distributions, variability, and trends, Elem Sci Anth, 6, 10, 2018.

Young, P., Archibald, A., Bowman, K., Lamarque, J.-F., Naik, V., Stevenson, D., Tilmes, S., Voulgarakis, A., Wild, O.,
870   Bergmann, D., et al.: Pre-industrial to end 21st century projections of tropospheric ozone from the Atmospheric Chemistry and Climate Model Intercomparison Project (ACCMIP), Atmospheric Chemistry and Physics, 13, 2063–2090, 2013.

Zhang, Y., Cooper, O. R., Gaudel, A., Thompson, A. M., Nédélec, P., Ogino, S.-Y., and West, J. J.: Tropospheric ozone change from 1980 to 2010 dominated by equatorward redistribution of emissions, Nature Geoscience, 9, 875–879, 2016.

Zhang, Y., West, J. J., Emmons, L. K., Flemming, J., Jonson, J. E., Lund, M. T., Sekiya, T., Sudo, K., Gaudel, A., Chang, K.-
875   L., et al.: Contributions of world regions to the global tropospheric ozone burden change from 1980 to 2010, Geophysical Research Letters, 48, e2020GL089 184, 2021.

Zhao, Y., Li, Y., Kumar, A., Ying, Q., Vandenberghe, F., and Kleeman, M. J.: Separately resolving NOx and VOC contributions to ozone formation, Atmospheric Environment, 285, 119 224, 2022.

Zheng, B., Tong, D., Li, M., Liu, F., Hong, C., Geng, G., Li, H., Li, X., Peng, L., Qi, J., et al.: Trends in China's anthropogenic emissions since 2010 as the consequence of clean air actions, Atmospheric Chemistry and Physics, 18, 14 095–14 111, 2018.

880
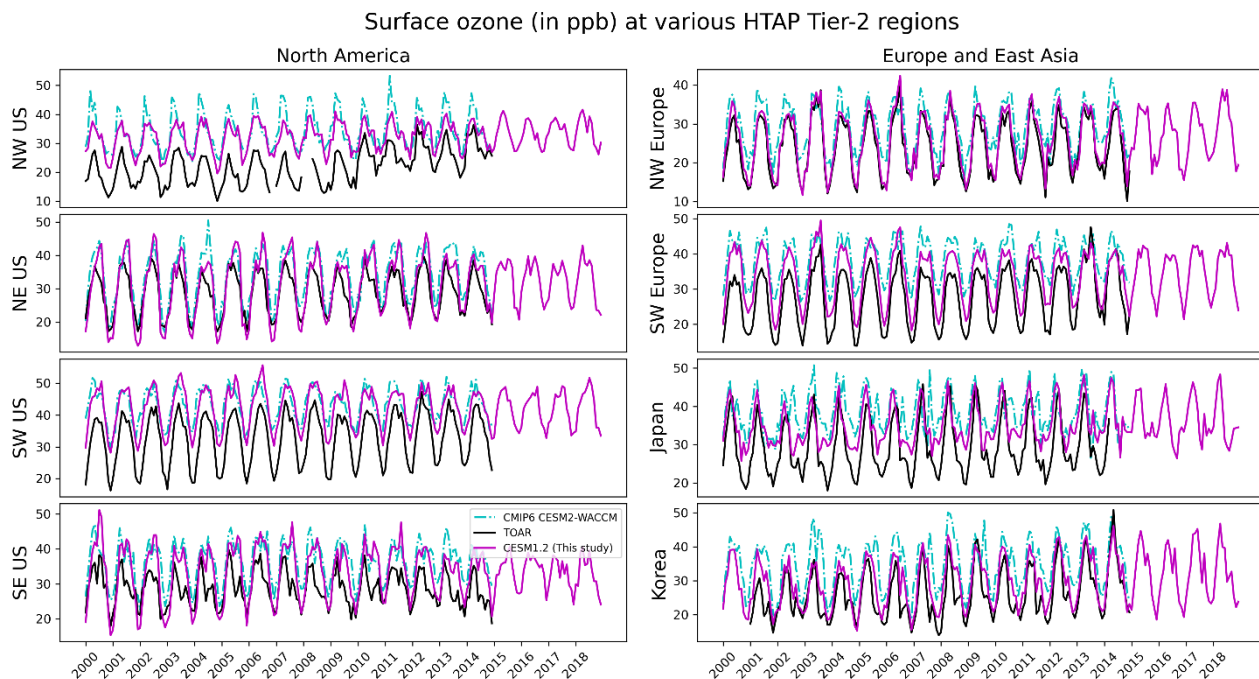
Fig. 1: Comparing the time-series of monthly mean surface ozone (in ppb) simulated over the 2000-2018 period in this study with the gridded observation dataset from TOAR available until 2014 (https://toar-data.fz-juelich.de/), at various regions defined by HTAP2 (Galmarini et al. 2017). The comparison is performed for simulated surface ozone values only over those grid cells where the TOAR data is available. Also shown is the comparison with the CESM2-WACCM6 model which is a CMIP6 ensemble member (also until 2014).
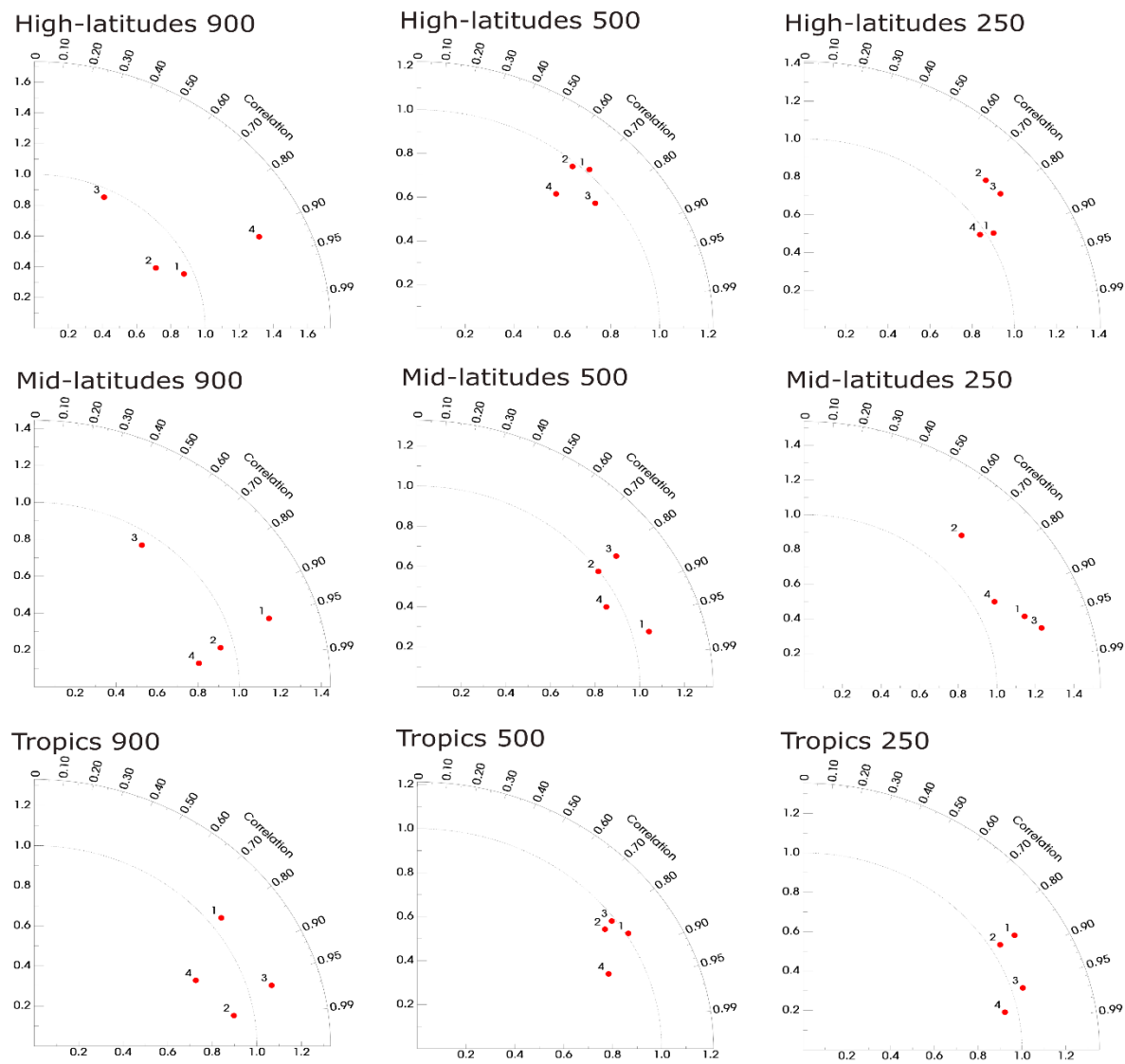
Fig. 2: Taylor diagram of comparisons between modelled monthly mean ozone climatology (2000-2018) and ozone sonde climatology (1995-2010) data from Tilmes et al. 2012 in the high Tropics (bottom), mid-latitudes (middle), and high latitudes (top) for three different altitude levels (900 hPa, 500 hPa and 250 hPa) in the troposphere. The x-axis shows the relative ozone normalized bias of the simulations compared to the observations, whereas the radiant in the y-axis describes the correlation coefficient of seasonal averaged ozone values between simulated and observed values. Numbers indicate different regions as difference in previous studies26,40. Bottom panels: 1-NH Subtropics; 2-W-Pacific/E-India Ocean; 3-equat. America; 4-Altantic/Africa; Middle panels: 1-Western Europe; 2-Eastern US; 3-Japan; 4-SH Mid Latitudes; Top panels: 1-NH Polar West; 2-NH Polar East; 3-Canada; 4-SH Polar.

900
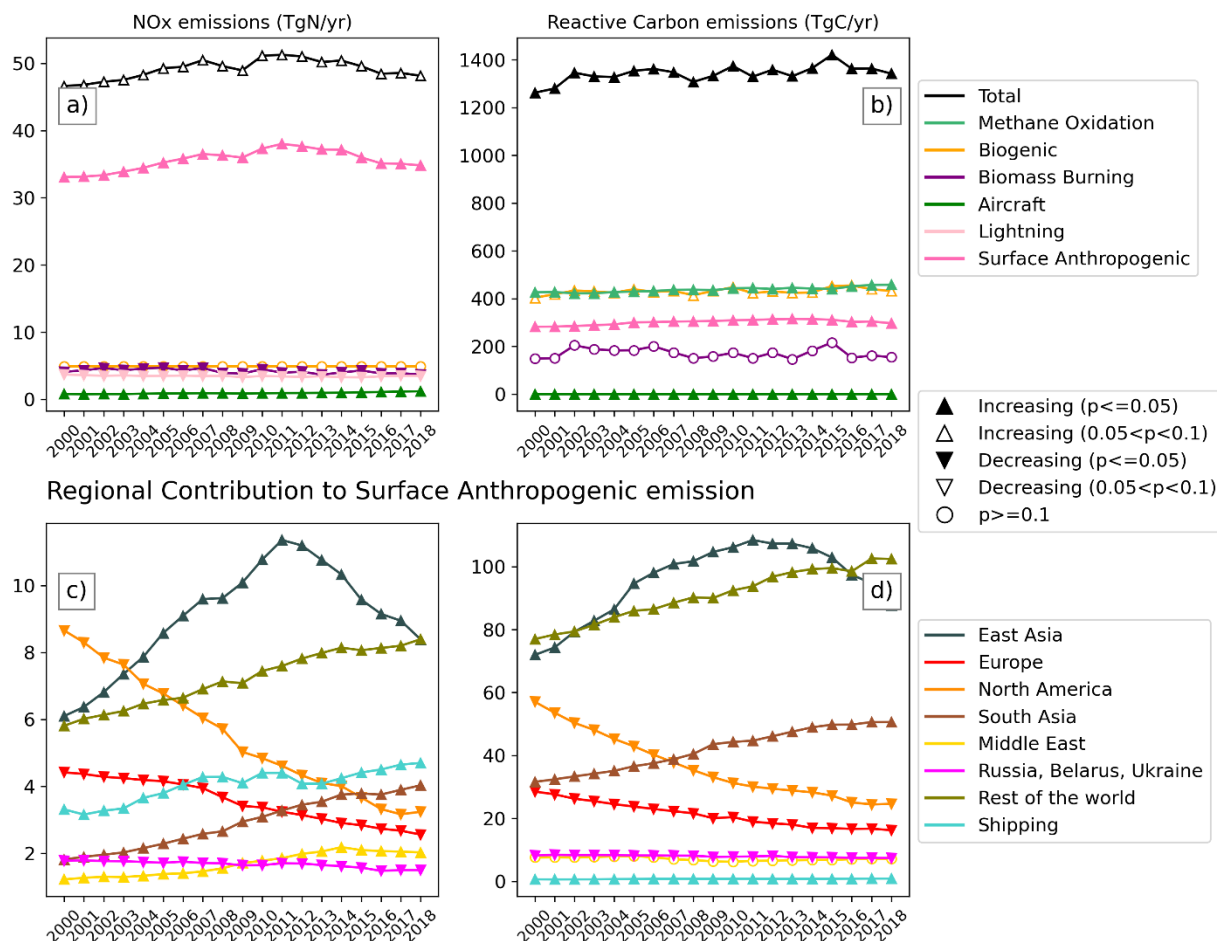
Fig. 3: Global annual emissions of ozone precursors from various sources used in this study. Left panels: NO_x emissions (in TgN/yr), right panels: reactive carbon emissions (TgC/yr). Bottom panels are the regional contributions to the Total Anthropogenic emission (dark pink line) shown in the top panels. The symbols indicate the sign and certainty of trend in the plotted quantity. The timeseries of relative contributions (in %) from each of the emission sectors to the total emissions is
905 provided in Supplementary Figure S3.

Fig. 4: a) Red line: Annually varying Methane mixing ratio (in ppm) prescribed in our model. Green line: Methane oxidation rate (in TgC/yr) simulated by our model. Magenta line: Lifetime of Methane (in years). b) Airmass weighted and CH4-reaction weighted tropospheric OH concentration (in 10^5 molec/cm^3). The symbols on the plotted timeseries indicate the sign of trend in the plotted quantity. The mean values, slope of trend, 95 % confidence interval and p-value for the 2000-2018 period are provided in Table S5.
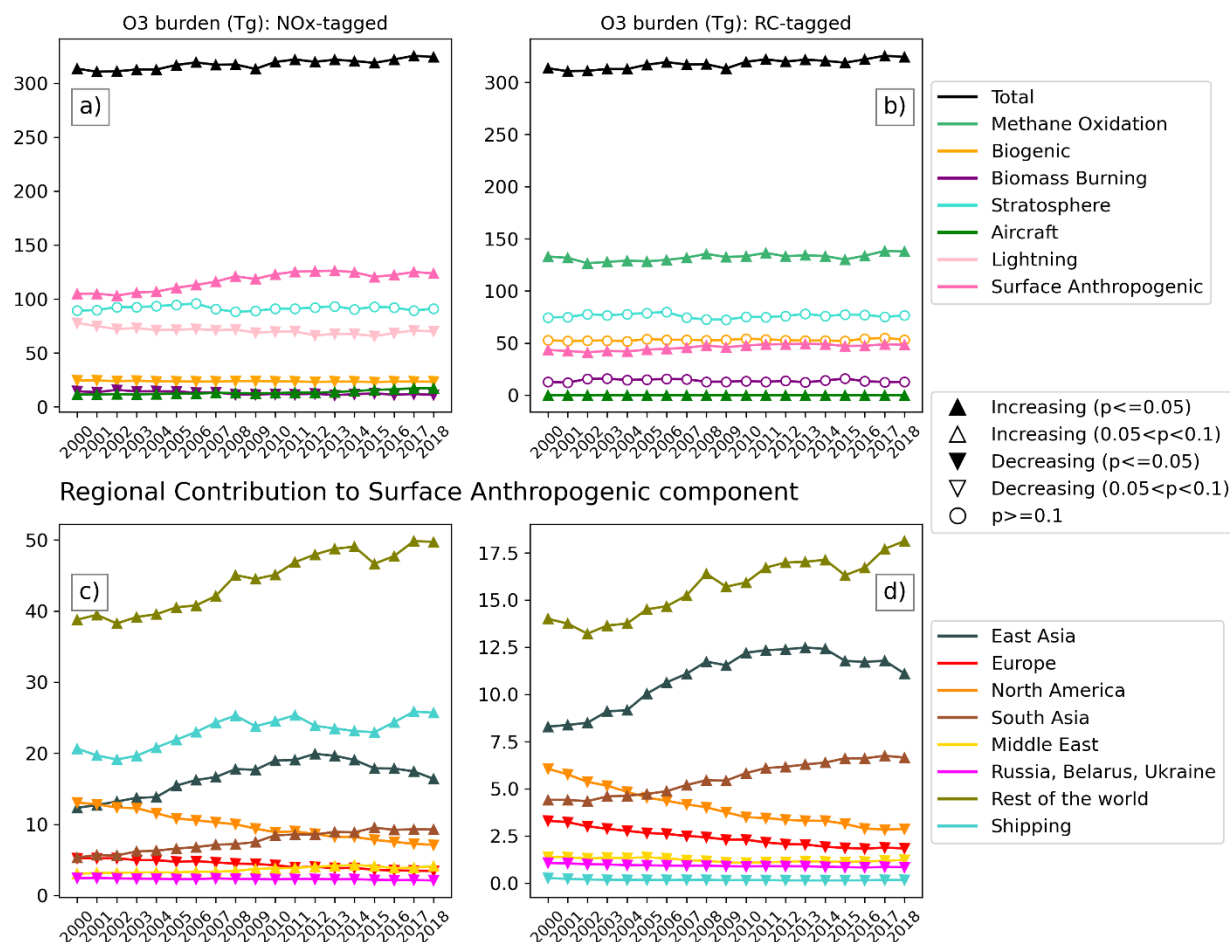
Fig. 5: Simulated global annual mean tropospheric ozone burden (in Tg O₃) time-series over the 2000-2018 period. Shown are the total simulated ozone burden (black line) and the contributions from the NOx-tagged (left panels) and RC-tagged (right panels) simulations. Bottom panels are the regional contributions to the Total Anthropogenic component (dark pink line) shown in the top panels. The symbols indicate the sign and certainty of trend in the plotted quantity. The timeseries of relative contributions (in %) from each of the emission sectors to the total emissions is provided in Supplementary Figure S5.
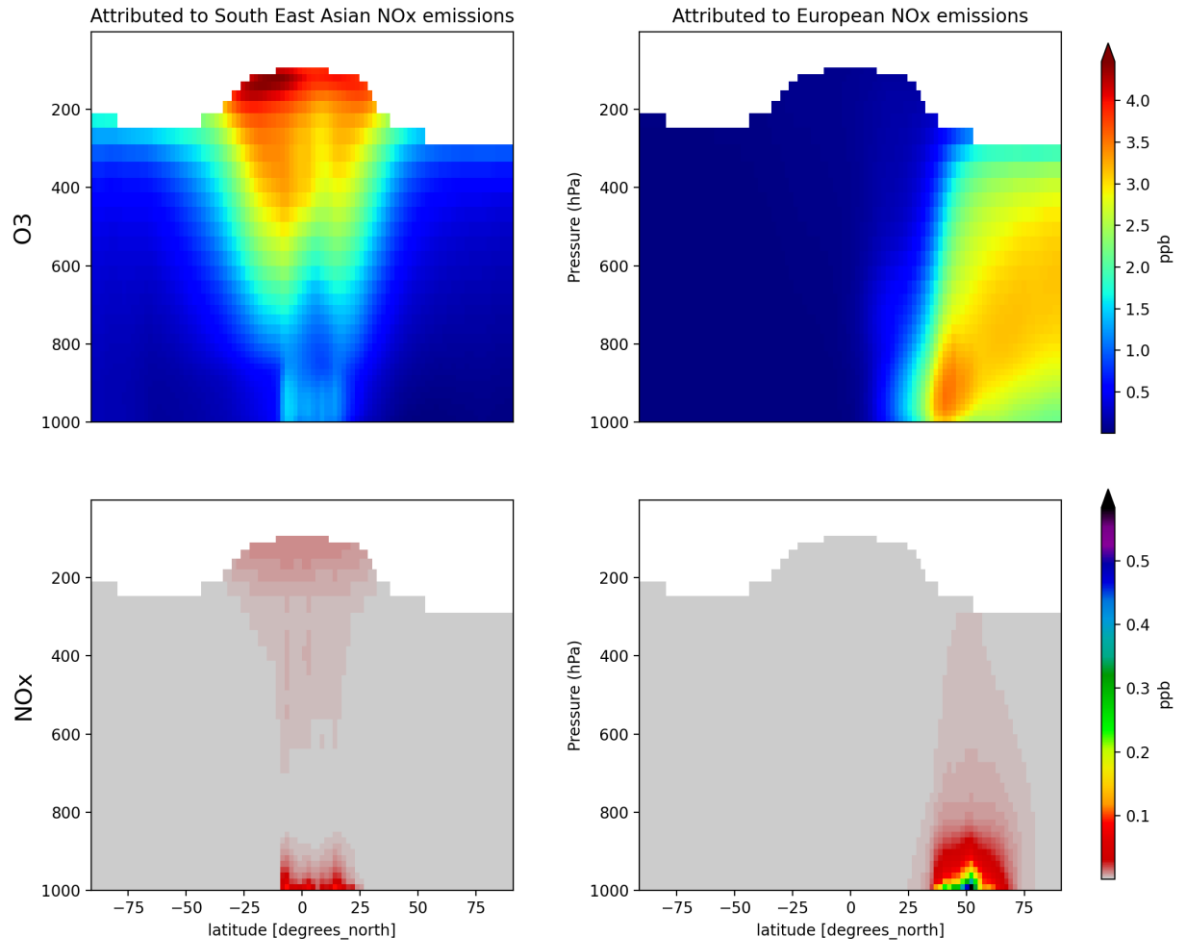
Fig. 6: Vertical profiles of zonal climatological (2000-2018) mean mixing ratio within the troposphere: O₃ (top panels) and
NOₓ (bottom panels) attributed to Southeast Asian (left panels) and European (right panels) anthropogenic NOₓ emissions.

Fig. 7: Time-series (2000-2018) of the Ozone production efficiency (OPE; in mol O_3/mol N: NOx-tagged left panels, mol O_3/mol C: RC-tagged right panels) of various ozone precursor emission regions/sectors tagged in this study. Bottom panels are the OPE values of regional anthropogenic emissions tagged in this study. The symbols indicate the sign and certainty of trend in the plotted quantity.
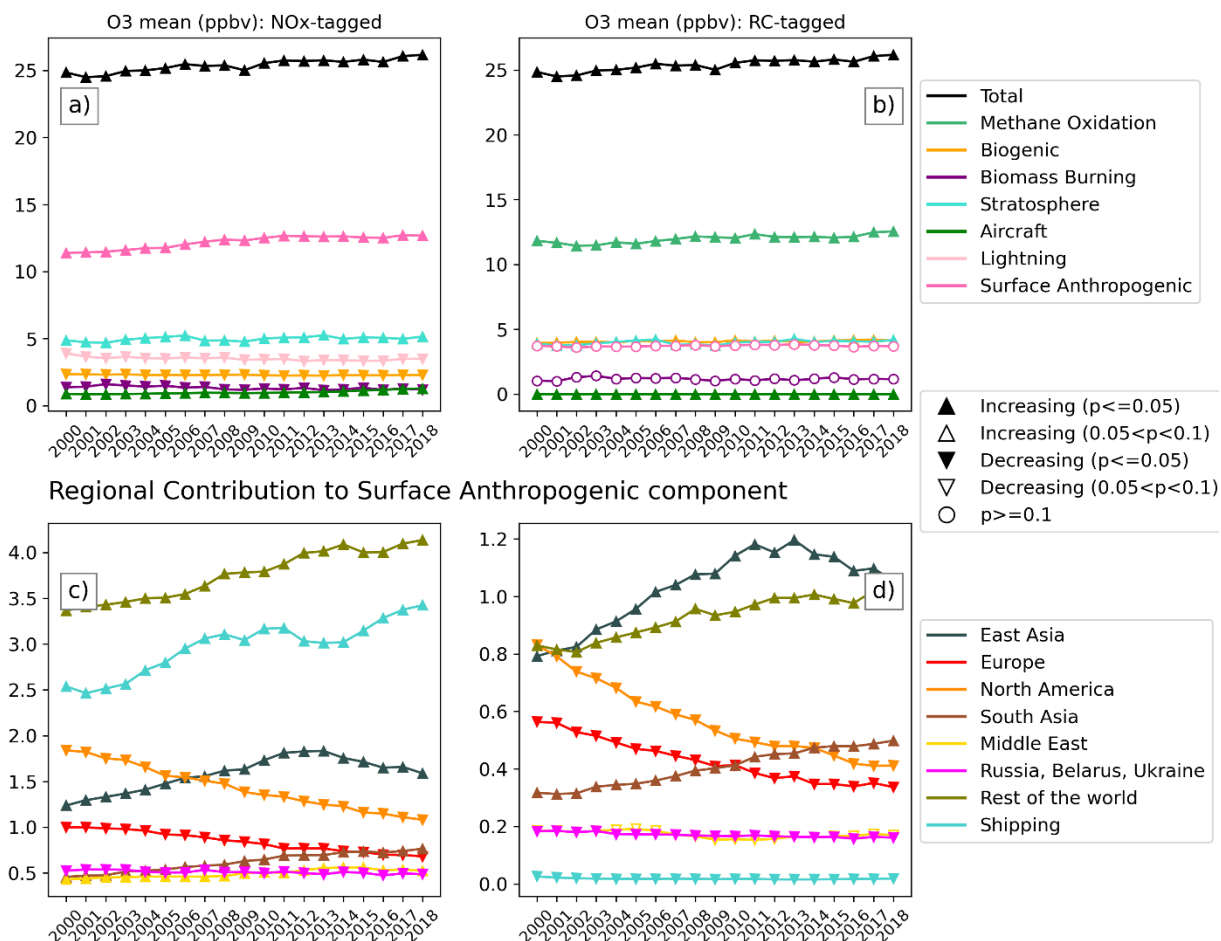
Fig. 8: Same as Figure 5, but for global annual area-weighted mean surface ozone (in ppb). The timeseries of relative contributions (in %) from each of the tagged components to the global annual area-weighted mean surface ozone is provided in Supplementary Figure S7.

930
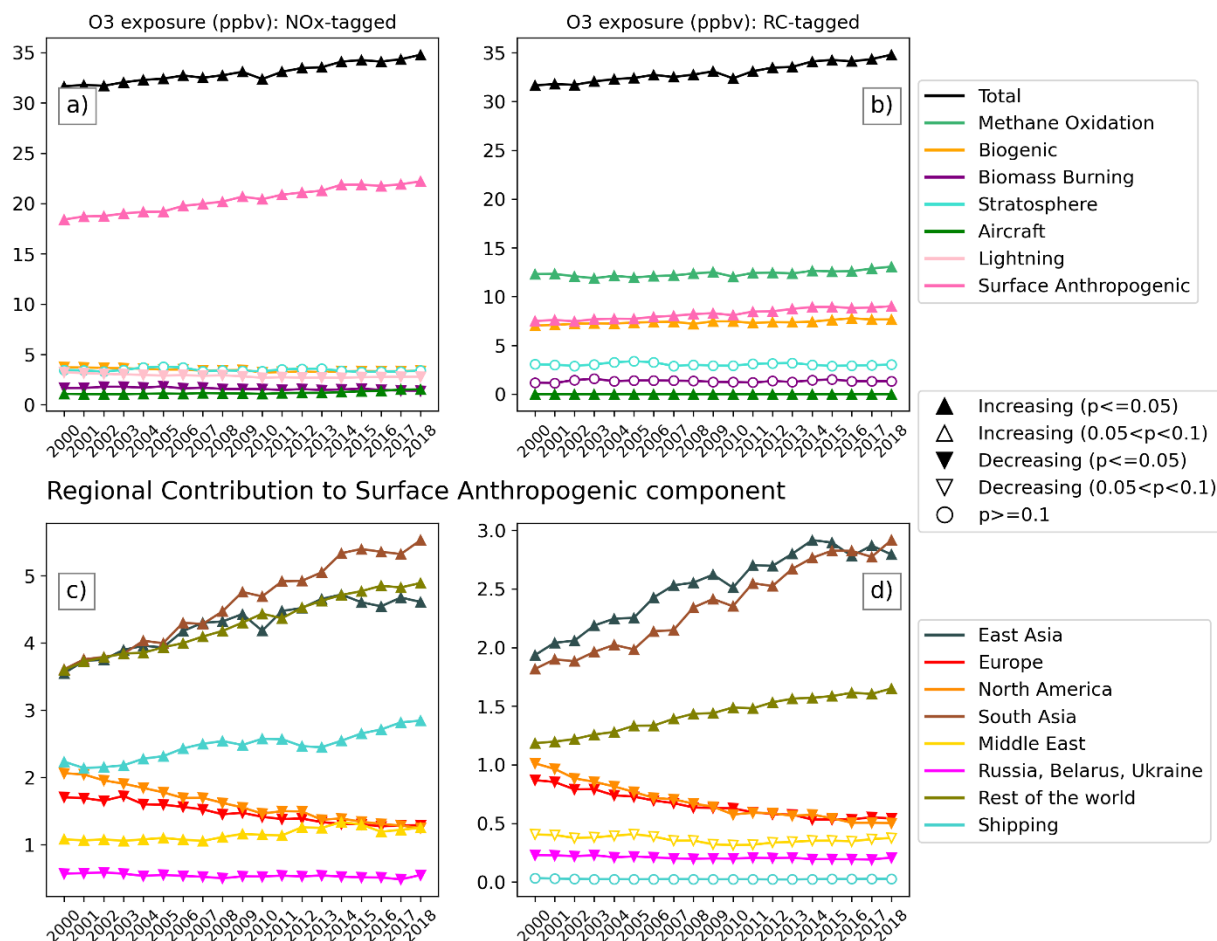
Fig. 9: Same as Figure 5, but for global annual population-weighted mean surface ozone (in ppb). The timeseries of relative contributions (in %) from each of the tagged components to the global annual population-weighted mean surface ozone is provided in Supplementary Figure S8.
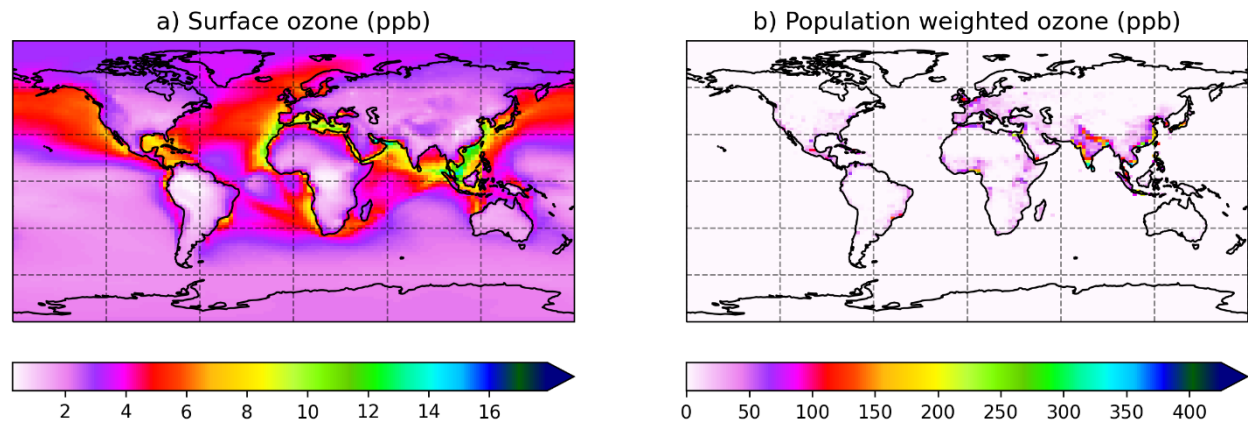
Fig. 10: Spatial distribution of climatological (2000-2018) annual mean O_3 attributed to NO_x emissions from international shipping (in ppbv): a) Surface ozone and b) Population weighted surface ozone.

Tag name	NOx-tagged	RC-tagged
HTAP Tier 1 regions		
International Shipping	Explicit	Explicit
North America	Explicit	Explicit
Europe	Explicit	Explicit
East Asia	Explicit	Explicit
South Asia	Explicit	Explicit
Russia, Belarus, Ukraine	Explicit	Explicit
Middle East	Explicit	Explicit
Southeast Asia	Explicit[S]->RoW	RoW
Northern Africa	Explicit[S]->RoW	RoW
Mexico and Central America	Explicit[S]->RoW	RoW
Central Asia	Explicit[S]->RoW	RoW
Pacific, Australia, and New Zealand	Southern Hemisphere Regions[S] ->RoW	RoW
Southern Africa	Southern Hemisphere Regions[S] ->RoW	RoW
South America	Southern Hemisphere Regions[S] ->RoW	RoW
Antarctica	Southern Hemisphere Regions[S] ->RoW	RoW
Arctic	Shipping	Shipping
Other tags		
Stratosphere[*]	Global	Global
Aircraft	Global	Global
Biogenic	Global	Global
Biomass Burning	Global	Global
NOx from Lightning	Global	N/A
RC from Methane Oxidation	N/A	Global
Extra Production	Global	Global

[S]Although explicitly tagged in the NOx-tagged simulation, these regions have been lumped into "Rest of the world" tag (RoW) used in this paper.
[*]NOx-tagged simulation attributes ozone to influx from the stratosphere (same as RC-tagged), and also to NO produced from oxidation of N_2O.

945

Table 1: List of tags used in this study. See Fig. S1 for a map of tagged regions considered in this study.

Source	Emissions (TgN/yr)	Tropospheric O$_3$ burden (TgO$_3$)	OPE (mol O$_3$ /mol N)	Surface mean (ppbv)	Population weighted mean (ppbv)
Total	49.12	317.93	N/A	25.39	33.01
Stratosphere	N/A	91.50 (28.78)	N/A	4.99 (19.65)	3.45 (10.44)
Aircraft	0.93 (1.90)	13.44 (4.23)	4.19	0.99 (3.91)	1.18 (3.59)
Biogenic	4.94 (10.05)	23.67 (7.44)	1.40	2.29 (9.01)	3.43 (10.40)
Biomass Burning	4.18 (8.52)	12.68 (3.99)	0.88	1.32 (5.20)	1.59 (4.82)
Lightning	3.47 (7.06)	70.51 (22.18)	5.93	3.51 (13.82)	2.86 (8.68)
Extra Production	N/A	0.97 (0.31)	N/A	0.08 (0.33)	0.11 (0.33)
Anthropogenic	35.60 (72.47)	116.94 (36.78)	0.96	12.20 (48.07)	20.38 (61.74)
Regional contribution to Anthropogenic component					
International Shipping	4.04 (8.22)	23.02 (7.24)	1.67	2.97 (11.69)	2.47 (7.47)
North America	5.51 (11.22)	9.79 (3.08)	0.54	1.43 (5.64)	1.61 (4.87)
Europe	3.54 (7.20)	4.36 (1.37)	0.36	0.84 (3.32)	1.47 (4.46)
East Asia	9.05 (18.43)	16.62 (5.23)	0.54	1.58 (6.23)	4.27 (12.92)
South Asia	2.91 (5.92)	7.64 (2.40)	0.78	0.62 (2.44)	4.60 (13.93)
Russia, Belarus, Ukraine	1.67 (3.39)	2.30 (0.72)	0.40	0.51 (2.01)	0.53 (1.62)
Middle East	1.68 (3.42)	3.64 (1.14)	0.64	0.49 (1.95)	1.15 (3.50)
Rest of the World	7.20 (14.66)	44.20 (13.90)	1.80	3.76 (14.80)	4.28 (12.97)

Table 2: Attribution of O$_3$ to NOx-tagged precursor emissions. 2000-2018 Mean contribution from NOx-tagged components to various metrics: Precursor emissions, tropospheric ozone burden, Ozone production efficiency, grid cell area weighted, and population weighted global mean surface ozone. In brackets is the percentage contribution to the total, wherever applicable.

Source	Emissions (TgN/yr^2)	Tropospheric O$_3$ burden (TgO$_3$/yr)	OPE ((mol O$_3$ /mol N)/yr)	Surface mean (ppbv/yr)	Population weighted mean (ppbv/yr)
Total	*0.13(0.29)	0.72(0.23)	N/A	0.08(0.30)	0.17(0.54)
Stratosphere	N/A	**1.83e-03 (2.06e-03)	N/A	0.02(0.32)	*-8.59e-03(-0.25)
Aircraft	0.02(2.52)	0.28(2.41)	**2.74e-03	0.02(2.18)	0.02(1.70)
Biogenic[1]	**0 (0)	-0.06(-0.26)	-3.74E-03	-3.86e-03(-0.16)	-0.02(-0.66)
Biomass Burning	-0.04(-0.91)	-0.20(-1.38)	-5.47E-03	-0.02(-1.14)	-0.02(-1.12)
Lightning	-0.01(-0.35)	-0.43(-0.56)	-0.01	-0.02(-0.44)	-0.03(-0.82)
Extra Production	N/A	6.61e-03(0.74)	N/A	3.62e-04(0.46)	7.16e-04(0.71)
Anthropogenic	0.19(0.59)	1.35(1.29)	7.35E-03	0.08(0.69)	0.22(1.19)
Regional contribution to Anthropogenic component					
International Shipping	0.08(2.47)	0.31(1.48)	-9.80E-03	0.05(1.92)	0.04(1.60)
North America	-0.33(-3.82)	-0.34(-2.59)	0.01	-0.04(-2.35)	-0.05(-2.24)
Europe	-0.11(-2.52)	-0.11(-2.12)	2.62E-03	-0.02(-1.97)	-0.03(-1.59)
East Asia	0.25(4.04)	0.40(3.29)	**2.27e-04	0.04(2.87)	0.06(1.74)
South Asia	0.13(7.41)	0.24(4.58)	-0.01	0.02(3.97)	0.11(3.09)
Russia, Belarus, Ukraine	-0.02(-0.87)	-0.02(-0.62)	1.34E-03	-2.64e-03 (-0.50)	-3.59e-03(-0.63)
Middle East	0.06(4.79)	0.07(2.26)	-0.01	6.97e-03(1.62)	0.01(1.12)
Rest of the World	0.15(2.58)	0.73(1.87)	-8.69E-03	0.05(1.35)	0.08(2.09)

*0.5<p<0.1 (medium certainty)
**p≥0.1 (low certainty)
[1]Since we prescribe an annually repeating seasonal cycle of biogenic/soil NO$_x$ emissions, the annual mean value is held constant leading to zero slope and p-value=1

Table 3: Theil-Sen estimator/slope of trends in contributions of NOx-tagged metrics, wherever applicable. Trend slope and p-value estimation has been summarized in section 2.3. The 95 % confidence interval and p-value for each of these estimated trends is provided in Table S1. In brackets is the trend in %/year. Note that this trend in %/year is the trend slope relative to the first value of the absolute contribution (for year 2000), and not to be confused with the relative contribution to the total as shown in Supplementary Figures S3, S5, S7 and S8.

Source	Emissions (TgC/yr)	Tropospheric O_3 burden (TgO3)	OPE (mol O_3 /mol C)	Surface mean (ppbv)	Population weighted mean (ppbv)
Total	1342.06	317.92	N/A	25.39	33.01
Stratosphere	N/A	76.04 (23.92)	N/A	3.99 (15.73)	3.05 (9.25)
Aircraft	0.24 (0.02)	0.03 (8.58e-03)	0.03	2.33e-03 (9.19e-03)	2.97e-03 (8.98e-03)
Biogenic	430.93 (32.11)	52.95 (16.66)	0.03	4.07 (16.04)	7.38 (22.37)
Biomass Burning	171.39 (12.77)	13.85 (4.36)	0.02	1.17 (4.62)	1.34 (4.06)
Methane oxidation	437.98 (32.63)	132.45 (41.66)	0.08	11.99 (47.22)	12.36 (37.46)
Extra Production	N/A	4.52 (1.42)	N/A	0.42 (1.67)	0.62 (1.88)
Anthropogenic	301.52 (22.47)	45.95 (14.45)	0.04	3.72 (14.67)	8.24 (24.96)
Regional contribution to Anthropogenic component					
International Shipping	0.76 (0.06)	0.17 (0.05)	0.06	0.02 (0.07)	0.02 (0.07)
North America	36.47 (2.72)	4.03 (1.27)	0.03	0.57 (2.24)	0.68 (2.07)
Europe	21.19 (1.58)	2.40 (0.75)	0.03	0.43 (1.69)	0.66 (1.99)
East Asia	95.36 (7.11)	10.87 (3.42)	0.03	1.03 (4.06)	2.52 (7.63)
South Asia	41.89 (3.12)	5.55 (1.74)	0.03	0.40 (1.59)	2.36 (7.15)
Russia, Belarus, Ukraine	7.97 (0.59)	0.92 (0.29)	0.03	0.17 (0.67)	0.21 (0.63)
Middle East	7.12 (0.53)	1.22 (0.38)	0.04	0.17 (0.68)	0.36 (1.10)
Rest of the World	90.77 (6.76)	15.65 (4.92)	0.04	0.93 (3.66)	1.43 (4.33)

Table 4: Same as Table 2 but for RC-tagged components

Source	Emissions (TgC/yr^2)	Tropospheric O$_3$ burden (TgO$_3$/yr)	OPE ((mol O$_3$/mol C)/yr)	Surface mean (ppbv/yr)	Population weighted mean (ppbv/yr)
Total	3.18(0.25)	0.71(0.23)	N/A	0.08(0.30)	0.17(0.54)
Stratosphere	N/A	**0.03(0.04)	N/A	0.02(0.40)	**-4.2e-03(-0.14)
Aircraft	3.9e-03(1.74)	4.66e-04(1.81)	**4.05e-05	3.60e-05(1.62)	4.65e-05(1.64)
Biogenic	*1.26(0.31)	**0.06(0.11)	**-1.38e-05	9.53e-03(0.24)	0.03(0.44)
Biomass Burning	**-0.77(-0.51)	**-0.08(-0.63)	**-2.89e-05	**-1.58e-03(-0.15)	**-1.72e-03(-0.14)
Methane oxidation	1.81(0.42)	0.44(0.33)	**-7.00e-05	0.05(0.42)	0.05(0.38)
Extra Production	N/A	0.02(0.54)	N/A	1.92e-03(0.48)	4.33e-03(0.76)
Anthropogenic	1.74(0.61)	0.45(1.03)	2.17e-04	**4.6e-03(0.12)	0.09(1.23)
Regional contribution to Anthropogenic component					
International Shipping	0.01(1.79)	-2.73e-03(-1.03)	-1.38e-03	-1.91e-04(-0.73)	**-7.06e-05(-0.22)
North America	-1.80(-3.16)	-0.17(-2.83)	1.58e-04	-0.02(-2.71)	-0.03(-2.58)
Europe	-0.72(-2.53)	-0.08(-2.53)	*-4.09e-05	-0.01(-2.46)	-0.02(-2.26)
East Asia	1.58(2.20)	0.23(2.77)	2.30e-04	0.02(2.91)	0.06(2.85)
South Asia	1.19(3.76)	0.15(3.51)	**-3.11e-05	0.01(3.54)	0.07(3.61)
Russia, Belarus, Ukraine	-0.06(-0.72)	-0.01(-0.98)	-1.03E-04	-1.3e-03(-0.71)	-1.87e-03(-0.82)
Middle East	**-0.05(-0.60)	-0.01(-1.01)	-1.42e-04	*-1.3e-03(-0.70)	*-2.62e-03(-0.65)
Rest of the World	1.50(1.95)	0.26(1.87)	**2.59e-05	0.01(1.62)	0.03(2.31)

*0.5<p<0.1 (medium certainty)

**p≥0.1 (low certainty)

Table 5: Same as Table 3 but for RC-tagged metrics. The 95 % confidence interval and p-value for each of these estimated trends is provided in Table S3.